공학박사 학위논문

A DEVELOPMENT OF ROBOT-ASSISTED LASER TREATMENT SYSTEM WITH CLINICAL TRIALS

로봇을 이용한 레이저 치료 자동화 시스템 및 임상시험

2017 년 2 월

서울대학교 대학원

협동과정 바이오엔지니어링 전공

임 형 우

A DEVELOPMENT OF ROBOT-ASSISTED LASER TREATMENT SYSTEM WITH CLINICAL TRIALS

로봇을 이용한 레이저 치료 자동화 시스템 및 임상시험

지도 교수 Sungwan Kim

이 논문을 공학박사 학위논문으로 제출함
2016 년 10 월

서울대학교 대학원
협동과정 바이오엔지니어링 전공
임 형 우

임형우의 공학박사 학위논문을 인준함
2016 년 12 월

위 원 장 박 광 석 (인)

부위원장 Sungwan Kim (인)

위 원 김 유 단 (인)

위 원 이 정 찬 (인)

위 원 김 인 영 (인)

Abstract

A DEVELOPMENT OF ROBOT-ASSISTED LASER TREATMENT SYSTEM WITH CLINICAL TRIALS

By

Hyoung-woo Lim

Interdisciplinary Program in Bioengineering

The Graduate School

Seoul National University

For optimal laser treatment, uniform distribution of laser delivery is essential. Research and development are conducted to compensate for the difficulties faced by physicians in tracking the exact location under irradiation by the laser because the duration of the laser flash is less than 300 ms, and the laser leaves no trace after irradiation. For laser treatment on large areas, physicians are

likely to lose focus owing to the simplicity and tediousness of the procedure along with fatigue because of prolonged hours of operation. To remedy these difficulties and achieve uniform laser delivery, two methods are proposed; one uses the automatic robot-assisted method and the other involves training physicians to increase their proficiency. Both methods are introduced here, but the automatic method is emphasized in this study.

A robot-assisted laser treatment system is composed of a commercial laser hair removal device, laser distance sensor, and high-resolution webcam attached at the end-effector of a six-axis robot arm. The software system is operated and provides visual information through a graphical user interface (GUI). The proposed system can detect an arbitrary shape of any size in red as a target for laser delivery and perform uniform distribution of laser irradiation on it. The system also contains a safety measurement system that both the patient and physician could pause and resume at will. The localization-error test and area-per-spot test produced satisfactory outcome averages of 1.04 mm error and 38.22 mm^2/spot, respectively. Clinical trials were conducted on six males aged 20-40 years. The treatment schedule comprised of four visits for treatment and the fifth visit only for a photograph session; subjects were photographed and shaved, and they received laser hair removal treatment on their laps (one by the system and the other by the physician) during the first through fourth visits at

two-week intervals. All subjects successfully completed the clinical trial with no noticeable or permanent side-effects. In terms of effectiveness comparison, the automatic system demonstrated an average hair removal rate of 49% (standard error of the mean [SEM]:4.0) while the physician achieved 29.5% (SEM: 4.0) under the same conditions. The average treatment duration and number of irradiation shots were 18 min, 30 s (SEM: 33 s) and 260 (SEM: 5.7), respectively, for the system and 3 min 11 s (SEM: 15 s) and 73 (SEM: 5.9), respectively, for physician-treatment. The system provided a near to idealistic number of irradiation shots, while the physician unsuccessfully completed the trials by providing an insufficient number of shots.

As most of laser treatment shares similar characteristics of difficulties, the proposed system is expected to be widely used in the field of low-level laser treatment.

Keywords: laser treatment, robot-assisted, laser delivery skills, uniform distribution of laser delivery

Student Number: 2011-23433

List of Tables

List of Figures

Contents

1. Introduction

It is extremely difficult for a physician to track the exact location of a laser irradiation spot by eye, because the laser pulse only lasts for between 3 and 400 ms,[1−3] and the practitioner can lose focus when treating a large area, such as the back, thighs, and hips. Often, failure to choose the correct laser intensity and dosage causes side effects such as pigment alteration, blistering, and erythema owing to the generation of excessive heat in the irradiated tissue.[4, 5] Insufficient delivery of laser light can also be problematic, leading to ineffective treatment or suboptimal results.[6, 7]

There are two methods to enhance laser delivery. One is to train physicians to achieve better results, and the other is to develop an automatic robot system with multiple sensors that can be programmed appropriately. Table 1.1 shows the strengths of both of these methods, which were both studied herein because of their necessity for achieving uniformly distributed laser delivery. We could statistically verify the differences between these two methods by investigating the diversity of laser delivery skills possessed by a physician. Based on these results, we developed a robot−assisted laser treatment system that could achieve uniform laser irradiation and maintain a user−defined rate of omission and redundancy by programming the robot to move in equal−sized steps.

We assumed that the system was only treating a two-dimensional (2D) space and that the patient was immobile. Currently, little attention has been paid to the necessity and the value of a uniformly distributed laser delivery. Our research is the first attempt to investigate this aim.

Table 1.1 Strengths and limitations for uniform laser treatment performed by trained physicians and robot-assisted laser treatment system.

Physicians with training	Robot-assisted treatment system*
Strengths	**Strengths**
- Almost no additional cost	- Utilization of the advantages of robots - Accuracy and precision of laser delivery - Automation - Programmability - Control of laser dosage - Visualization of progress and completion - Wide application in the field of laser treatment (versatility)
Limitations	**Limitations**
- Existence of human errors - Diversity of skills among physicians - Downfall of focus and fatigue on physicians - Not a permanent resolution	- Initial development cost - Operation cost

* Physicians are supervised.

1.1 History of laser treatment and medical robots

In 1917, Albert Einstein's theory of stimulated radiant energy sparked research for monochromatic radiation of spectra of molecules, which ultimately led to collaboration between physicists and engineers and the invention of the first laser in 1960s[8]. In fact, the R&D on light amplification has longer history than its first invention but Charles H. Townes (1915-2015) is widely recognized for opening up the era of amplification through his invention of MASER (Microwave Amplification by Stimulated Emission of Radiation) in 1953. In 1960, Theodore H. Maiman (1927-2007) of Hughes Corporation Research Laboratory presented the first functional optical ruby maser excited by a xenon flash lamp which illuminated pulse of 693 nm. A deep red light of less than 1 ms in duration and a power output of about a 100 million W/pulse[9]. It was the first invention of what is now called LASER (Light Amplification by Stimulated Emission of Radiation)(Figure 1.1 (a)). Nowadays, various other laser modules such as Q-switch, semiconductor diode, Nd-YAG, Er-YAG, CO_2 and many more exists and are used in the field of medicine including dermatology[8].

The current most renowned laser clinical laboratories to name a few are Beckman Laser Institute, Wellman Center for

Photomedicine, Laser Biology Research Laboratory and Oregon Medical Laser Center. These research & development centers are all located in the USA but the first attempt to study and clinical trial of phototherapy was conducted in Netherland. A Dutch scientist and physician Niels Ryberg Finsen (1860 −1904) saw the potential of phototherapy (Figure 1.1 (b)) in the field of medicine and used it to treat Lupus vulgaris. He was awarded Nobel Prize in Physiology in 1903 for his contribution to the treatment of lupus vulgaris, with concentrated light radiation.

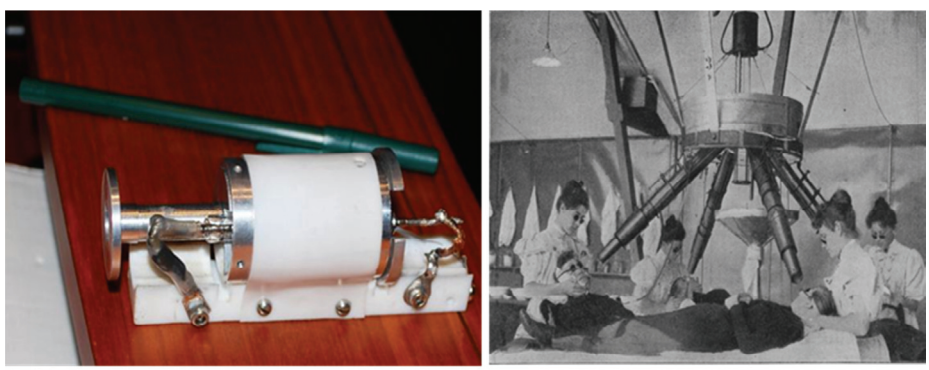

(a) (b)

Figure 1.1 Early models of devices. (a) Maiman's original ruby laser (excerpted from Wikipedia) (b) Finsen's phototherapy using the apparatus for localized electrophototherapy (excerpted from gemstoneuniverse.com).

In 1963, Leon Goldman saw immense potential on the invention of ruby laser by Maiman. Goldman and his colleague quickly adopted the works of Maiman in the field of dermatology and published effects of laser on selective destruction of pigmented structures of

the skin including hair follicles by the pulse from ruby laser. Goldman continued his work on pulsed laser and its clinical effect with various lasers to treat nevi, melanomas, and tattoo removal.

Lasers have been also used for photocoagulation and photoexcision through continuous wave form. Cancer cells were removed through continuous wave of laser (photoexcision) which conventional surgical instruments could not achieve. Laser types such as CO_2, Nd−YAG, and argon laser are used in this field and were developed in order, respectively.

In the early 1980s, R. Rox Anderson and John A. Parrish, from the department of dermatology in Harvard medical school developed the theory of selective photothermolysis which explained that the prolonged exposure to the laser energy is responsible for the collateral thermal damage in the surrounding tissue of the target chromophore. This principle and concept of understanding thermal relaxation time of laser therapy revolutionized the field of cutaneous laser therapy which inventors and engineers started to adopt this principle by designing the laser device by manipulating pulse duration, wavelength, spot size, fluence to reduce collateral damage on the surrounding chromophores; enabling to damage only the desired chromophores. This approach introduced a new field of market for treating cutaneous lesions, especially in tattoo removal and hair removal.

Historically and recently, robots in medicine have been mostly used in tele-manipulators, which receives the surgeon's action from one end to control the "effector" on the other end. Several medical robot types exists and they include but not limited to surgical robots, rehabilitation robots, bio-robots, telepresence robots, pharmacy automation and disinfection robot.

In 1985, robots were first introduced by Kwoh et al to perform neurosurgical biopsies with greater precision. This robot was the "Puma560" from Unimation (Figure 1.2(a)). 3 years later, a robot system designed for transurethral resection was developed and was named PROBOT. Next, Integrated Surgical Systems developed "ROBODOC" (Figure 1.2(b)) to move the femur during hip replacement surgeries and it became the first robot to be approved by the FDA.

Various commercial companies have developed surgical robotic systems and nowadays, numerous projects on new robots in medicine are launched. Followings are cases of significant and well known cases of robots in medicine

AESOP® Endoscope Positioner was developed by Computer Motion, Inc. (Figure 1.2(c)) is a voice-activated robotic system for endoscopic surgery which was approved by the FDA in 1993. Intuitive Surgical, Inc. designs and builds the da Vinci Surgical Systems, (Figure 1.2(d)) a platform for robotically assisted

minimally invasive surgery, is arguably the most commercially successful case of robots in medicine. In 2001, Computer Motion created SOCRATES™ Robotic Tele-collaboration System which includes integrated telecommunication apparatus to provide remote surgical tele-collaboration. This system was the world premier case of transatlantic tele-surgery and quickly gained the attention of the media.

Many more application of robots and its instruments in the medical field are researched and developed around the world. Table 1.1 describes the strength and limitations for surgeries done by humans and assisting robot. The designers of the robot or the inventors of the system should always acknowledge these pros and cons prior to building one to clarify the necessity of their creation. Forerunners and pioneers takes great amount of risk but enjoys their reward through success of their business model and patents protection. Robotics in medicine are high valued industry that second runners often faced with difficulties. Therefore, understanding and grabbing the new necessities and it's usage from the field are essential to become the forerunner and the success of the business.

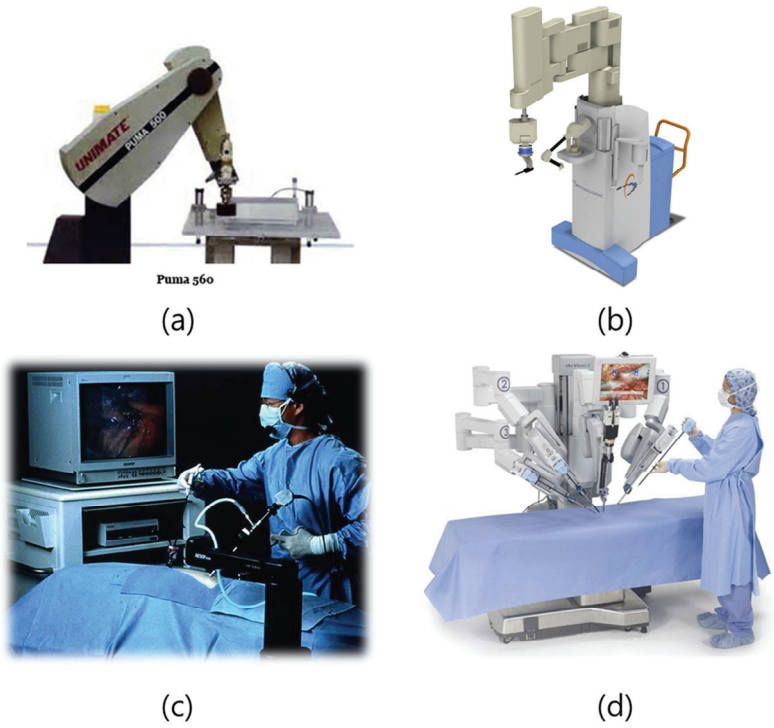

Figure 1.2 Various robots in the field of medicine. (a) PUMA 560 for neurosurgical biopsies (hoffroboticsurgery.com), (b) ROBODOC for hip replacement surgery (medicalgrapevineasia.com)
(c) Automated Endoscopic System for Optimal Positioning (AESOP) robotic system (urologiasc.com)
(d) da Vinci® Surgical System for minimally invasive surgery (intuitivesurgical.com).

Table 1.2 Strengths and limitations for surgeries done by humans and assisting robots.

Humans	Robots
Strengths	**Strengths**
− Strong hand−eye coordination	− Good geometric accuracy
− Dexterous (at human scale)	− Stable and untiring
− Flexible and adaptable	− Can be designed for a wide range of scales
− Can integrate extensive and diverse information	− May be sterilized
− Able to use qualitative information	− Resistant to radiation and infection
− Good judgement	− Can use diverse sensors (chemical, force, acoustic, etc.) in control
− easy to instruct and debrief	
Limitations	**Limitations**
− Limited dexterity outside natural scale	− Poor judgement
− Prone to tremor and fatigue	− Limited dexterity and hand−eye coordination
− Limited geometric accuracy	− Limited to relatively simple procedures
− Limited ability to use quantitative information	− Expensive
− Large operating room space requirement	− Technology in flux
− Limited sterility	− Difficult to construct and debug
− Susceptible to radiation and infection	

*Source: Table from Howe, RD, Matsuoka, Y. robotics for surgery. Annual Review

1.2. Laser treatment and laser hair removal

Lasers are artificial light sources that are tuned to emit light of highly specific wavelengths, allowing light to be focused into powerful beams. In medicine, lasers offer the ability to work precisely; the treatment is focused on a small area and damages less of the surrounding tissue. Patients who have laser therapy experience less pain, swelling, and scarring than those who undergo traditional alternatives.[10] Laser treatments are also used cosmetically to lessen the appearance of wrinkles and blemishes and to remove warts, moles, tattoos and hair. Different lasers are used for different procedures, but those used cosmetically all rely on the principle of selective photothermolysis and often share similar properties, such as low intensity (low-power) and direct contact between the laser beam and the skin.

The effects of applying laser beams to live tissue differ depending on the absorption characteristics of the tissue components. The main absorbing skin chromophores are water, melanin, and hemoglobin, which have different absorption spectra.[11-14] The principle of selective photothermolysis involves tuning the wavelength of a laser to target the absorption range of the desired

skin chromophore and thereby affect the target chromophore. The effectiveness of the treatment depends on parameters such as the laser wavelength, power, spot size, exposure time, and fluence. Therefore, the delivery of an appropriate dose of laser light is paramount for safe and effective treatment. Areas that are omitted because of poor laser delivery technique will have sub-optimal results,[15] and paradoxical hypertrichosis can also occur after treatment involving poor laser delivery. The intensity of the laser pulse is not evenly distributed throughout the laser output window but has a normal distribution (bell curve); the energy is drastically reduced as the distance from the center increases. Therefore, a large omission percentage can not only leave behind untreated hairs but can also stimulate the growth of thicker hair in some cases.[16]

The best laser treatment results are achieved the laser beam is distributed as uniformly as possible on a patient's skin surface. While the principle of selective photothermolysis means that irradiation will selectively damage the hair follicles if the laser is uniformly irradiated, physicians often do not achieve uniform laser distributions. Moreover, the location of hairs cannot be distinguished with naked eyes during the laser treatment, since the treatment takes place after a complete shave.

We have developed a laser treatment system to achieve uniformly distributed laser irradiation using a robot-assisted method, which

can be applied in any laser treatment in which a uniform laser distribution benefits the patient. However, our system was tuned specifically for laser hair removal to match a clinical trial that will test the effectiveness of the proposed system and the effects of uniform distribution of laser delivery on laser hair removal.[17−20]

A laser hair removal (LHR) practice based on the selective photothermolysis principle is economical, less painful to the patients, and time efficient compared with other hair removal practices, such as electrolysis/thermolysis, tweezing, or shaving.[10] These methods do not provide a permanent solution to hair removal.[21, 22] Moreover, various types of lasers used for LHR, including alexandrite, diode, Nd−YAG, ruby, and intense pulsed light (IPL) have been approved by the United States Food and Drug Administration (FDA) and have all demonstrated effectiveness and safety when applied to LHR treatment.[15]

Figure 1.3 depicts the clinical settings and laser irradiation delivery methods used by physicians. A laser pulse is released from the LHR device when the light output window is in direct contact with the skin. It is very difficult to trace the exact location of the laser focus regardless of the pulse duration. There are two manual methods of laser delivery; ‘pick and place’ and ‘sliding,' as shown in Figure 1.4.

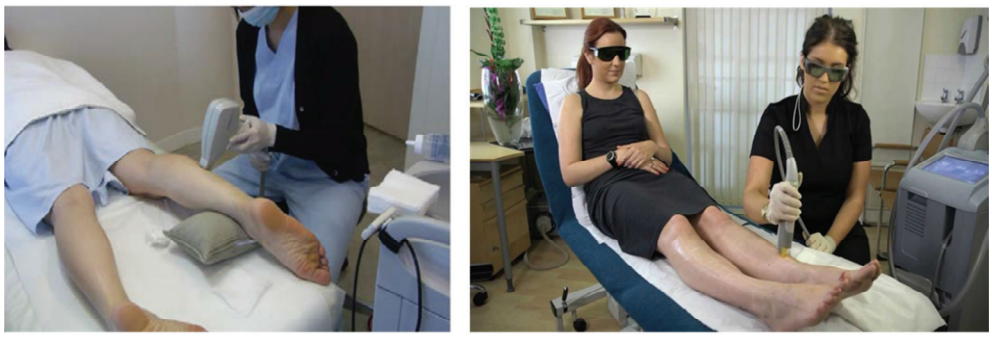

a b

Figure 1.3 Various laser treatment conducted in clinics; (a) laser hair removal practiced in JMO Clinic, (b) hyperpigmentation laser treatment from Cutera (excerpted from Cutera).

Physicians tend to prefer the easier maneuverability of the 'sliding' method over 'pick and place.' 'Sliding' involves the physician holding the laser end-piece with the light output window of the end-piece in direct contact with the skin, and moving the end-piece along as the laser pulse is released. 'Pick and place' has an extra movement (the 'pick' movement) which creates more muscle fatigue than the 'sliding' method, but allows the irradiation site to be more easily predicted. The hydrogel that is used during the delivery to reduce friction and for cooling can provide an approximate location of the laser irradiation site, but it remains difficult to realize the irradiated location regardless of the method used.

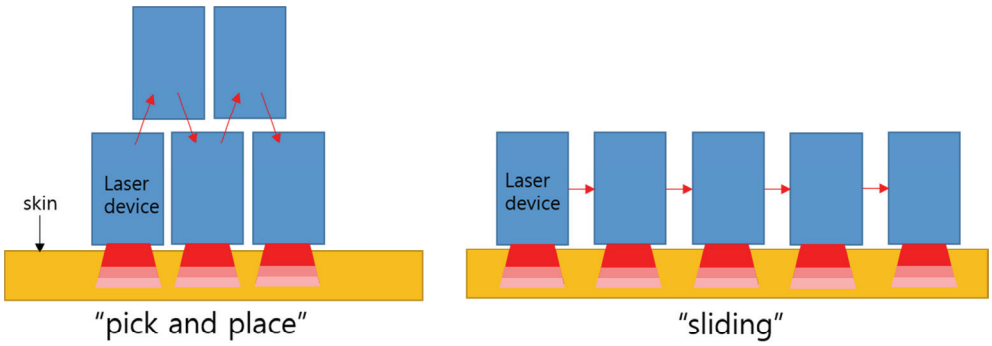

Figure 1.4 Illustration of "pick and place" and "sliding" mode. One is to make attachement and detachment motion while the other is releasing laser irradiation on the way.

1.3. Diversity of laser delivery skills among physicians

Many laser devices for skin treatment have been developed but the variations in the technical skill of physicians for laser treatment delivery have not been evaluated. We evaluated the differences in omission and overlap percentages during simulated laser treatments[23]. A laser beam detection kit was developed to record and collect laser irradiation from a diode laser device (Lumenis, Santa Clara, USA) used in professional clinic. Eight physicians were recruited to perform 80 trials of laser delivery simulation. The process was filmed through a webcam that is located inside the

laser beam detection kit and evaluated through image processing and computer calculation. The laser was irradiated on the flat surface of silicon sheet which mimic the friction of the skin. Human body parts are not flat but the flat surface was chosen to provide idealistic condition to perform uniform distribution of laser delivery. It is no question that it will be much harder to perform the goal in contoured surface than flat.

The uniform distribution of laser delivery is paramount on safe and effective laser treatment. However, it was found from the study on the evaluation of physicians' laser delivery performance using a laser beam detection kit (Figure 1.5 and 1.6) that treatment skill differed both in terms of inter- and intra- among the individuals as shown on Figure 1.7 and Figure 1.8. The area of the rectangular target was 15,000 mm^2 (150 mm × 100 mm). The treated area was defined as any area within the rectangular target that had been irradiated more than once. The overlapped area was defined as the area within the rectangular target that had been irradiated more than twice. Statistical validation of the data was performed through the ANOVA test, the Kruskal-Wallis test, and Mann-Whitney test with post-hoc Bonferroni adjustment analysis. The difference between the skills of clinics was also analyzed using the independent t-test and Mann-Whitney test. The test result for significant difference was set by the p-value less than 0.05. The primary effectiveness assessment are defined by the percentage of

untreated percentage (δ_0), redundantly treated percentage (δ_z), which are shown in equation 1.1 and 1.2,

$$\delta_0[\%] = \frac{Area\ of\ the\ rectangular\ target - Treated\ area}{Area\ of\ the\ rectangular\ target} \times 100 \qquad (1.1)$$

$$\delta_z[\%] = \frac{Overlapped\ area}{Area\ of\ the\ rectangular\ target} \times 100 \qquad (1.2)$$

This study is crucial since the diversity of delivery skills signifies non-uniform distribution of laser delivery that directly relates to efficacy of the treatment which leads to suboptimal result or overexposure of dosage.

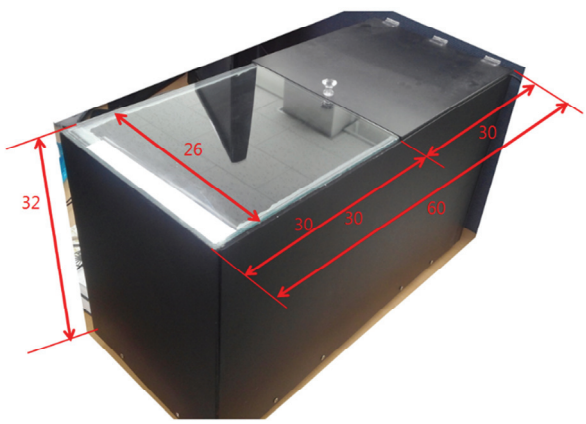

Figure 1.5 The exterior of the laser beam detection kit.

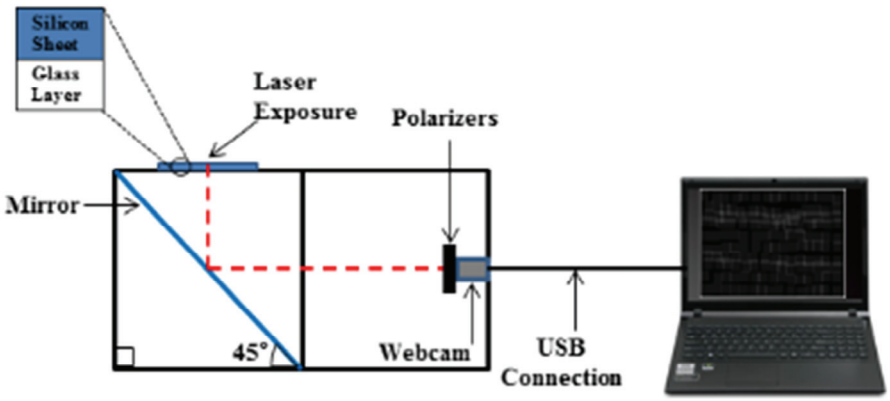

Figure 1.6 The interior design of the laser beam detection kit.

In this study, we found that physicians who generally had higher omission rates had lower overlap rates and vice versa. This means that without special training or feedback, physicians may either perform repeated passes to avoid omission, decrease the number of passes to avoid overlap, or shorten the treatment. All of the physicians were asked to do their best to deliver uniform distribution of laser delivery. If it were possible for a human to perform uniform distribution, both the omission and overlap percentage will be low, human error is unavoidable. Figure 1.7 (a) is not an idealistic case but comparably has moderate omission and overlap percentage, Figure 1.7 (b) is the case high percentage of overlap and lower percentage of omission. The physicians focused on lowering omission percentage but the overlap percentage was significantly high. Not to mention the duration of laser delivery and number of shots were significantly high compared to other cases.

Figure 1.7 (c) is the case when the physician starts to increase the overlap percentage by the end of the test. Figure 1.7 (d) is the case which rows are quite evenly distributed but columns are not. There are many more variations among the physicians and each physicians tends to display distinct characteristics.

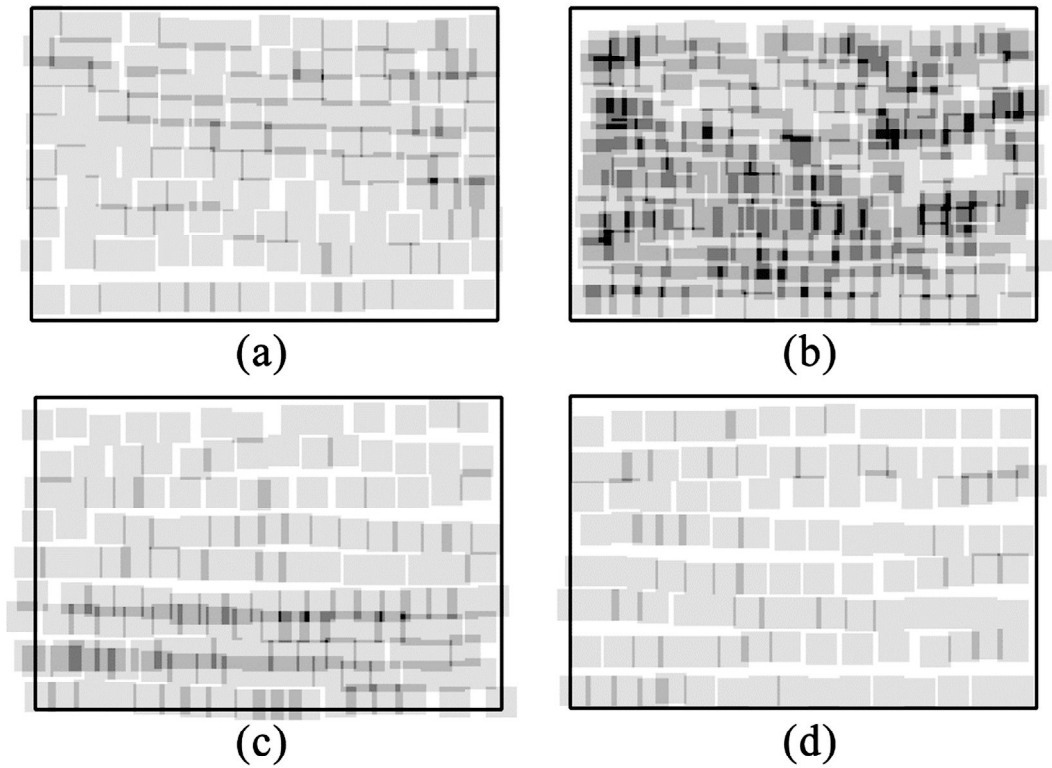

Figure 1.7 The performance of four different physicians. Diversity among physicians' delivery skill are shown through experiment. (a) moderate case of omission and overlap percentage (b) High percentage of overlap (c) increase of overlap by the end (d) relatively uniform in rows but high omission in column.

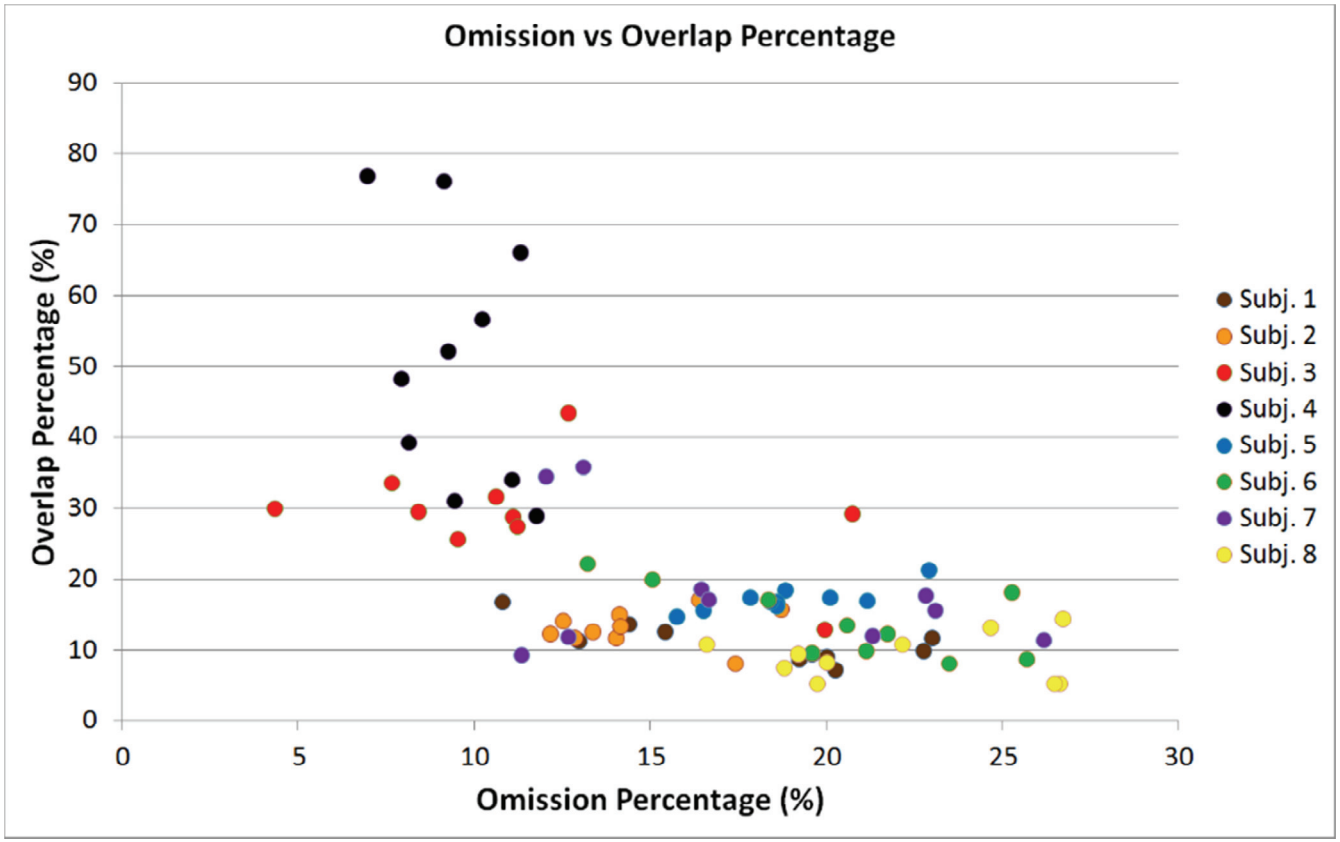

Figure 1.8 Omission and overlap percentages for each physician. Graph showing the distribution of 80 trials.

1.4. Robot-assisted laser treatment system

In technical point of view, a novel method that can perform uniform distribution of laser delivery is required to be developed to control omission and overlap. With the help accurate and precise sensors and 6-axis robot arm, the drawbacks of currently conventional non-uniform laser delivery can be overcame. The present study is focused on achieving a safe and effective laser treatment system using uniform laser delivery and through achieving the goal, this system is aimed to compensate the difficulties of physicians. The omission and overlap percentage can be controlled by user. It is a visually guided, robot-assisted system that automatically detects the target and performs the "pick and place" motion. A red-colored marker is employed as a target area to evaluate the performance of the system, and a clinical trial involving human subjects was conducted to verify the safety and efficacy.

2. Materials and methods

2.1. System overview

This study investigated a safe and effective laser delivery system that can achieve uniformly distributed laser irradiation. The new system is a visually guided, robot-assisted system that automatically detects the laser irradiation target and performs the "pick and place" motion on the target. A red-colored object is employed as a target to evaluate the performance of the system. The system was designed to conduct the clinical trial as final proof of principle.

The robot receives coordinate data regarding the external environment through a vision sensor (webcam) and a laser distance sensor (Figure 2.1). The visual and distance information from these two sensors is used to compute the end-effector pose with respect to an object observed by the camera and measured by the laser distance sensor. These two sensors are attached to the end-effector of the robot, and the desired coordinates of camera and robot's end-effector can be determined from calibration and coordinate mapping. The sensors measure their data in relation to the end-effector's location. The vision system can track the location of the target within its view and the laser distance sensor

can measure the distance between the sensor and the target. The sensors send their data to the computer, which sends commands to the robot controller. The controller provides the desired task frame velocities and task frame pose of the robot, then the robot's joints rotate as commanded. Overall, the data input from these sensors is used as coordinate data for the end-effector.

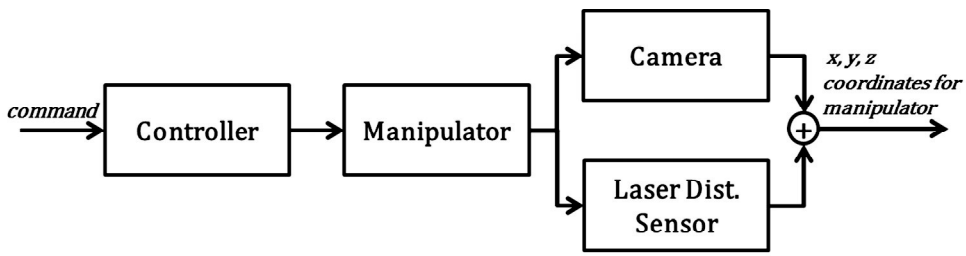

Figure 2.1 General scheme of robot control for integrating vision and laser sensor on the system.

2.1.1 Hardware overview

A series of development phases were undertaken before the final version was achieved. The following brief explanations give details of each version:

i) Version 0.5 (Figure 2.2); the camera and ultrasound (U/S) sensor were attached and tested in combination, and the best site for their attachment was chosen. Data acquisition devices (DAQs) were tested for receiving and transmitting the data values from the sensors to the computer. The initial stages of image processing such as extracting camera coordinates of interest were implemented. In this stage, the target was assumed to be a flat 2D surface, and the patient was immobile.

ii) Version 0.8 (Figure 2.3); with the knowledge gained from Version 0.5, the fixing structure was designed and made to fix the laser device, camera, and U/S sensor rigidly and compactly. In this version, the three devices were integrated as a single complimentary set. The software was designed to command the system through a graphical user interface (GUI), and the operator received visual information through a monitor. Work to plan and map coordinates between the camera and the robot coordinate was begun at this stage. A work order for the 'pick and place' movement and an algorithm for coordinate mapping were programmed. The

target's figure was limited to a rectangle, and the four corners of the rectangle were automatically detected. However, some changes had to be made during optimization of the system for better performance and to serve a new goal.

iii) Version 0.9 (Figure 2.4); this version was made to fulfill the goal of the clinical trial of the system at the end of the development. It was quickly realized that the U/S sensor was not accurate enough to measure the distance. Thus, it was replaced with 1D laser distance sensor. Arbitrary shape detection functions were added to the software, and the GUI was revised to be more concise and simple. The clinical trial focused on the differences in the number of irradiated shots and compared the hair removal rate between the proposed system and the physician-directed result. A brief history of the development of the system is provided in Figure 2.5. The development of the hardware and software is also shown in Figure 2.5.

iv) Version 1.0 (Figure 2.6); The overall hardware component specifications of version 1.0 are shown in Figure 2.6 and listed in Table 2.1. The proposed system's exterior appearance is shown in Fig. 2.7.

Webcam and laser device on robot

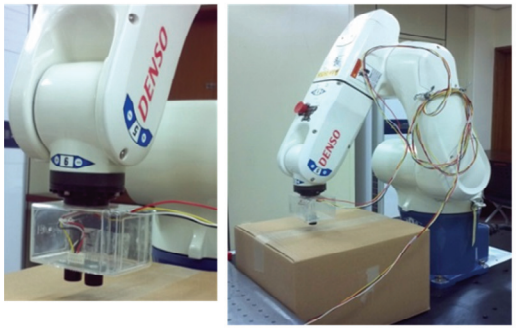

U/S sensor for distance detection

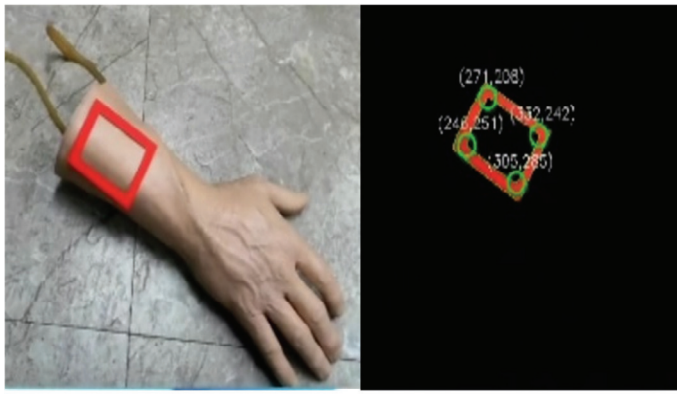

Coordinate extraction through image processing

Figure 2.2 Development of Version 0.5.

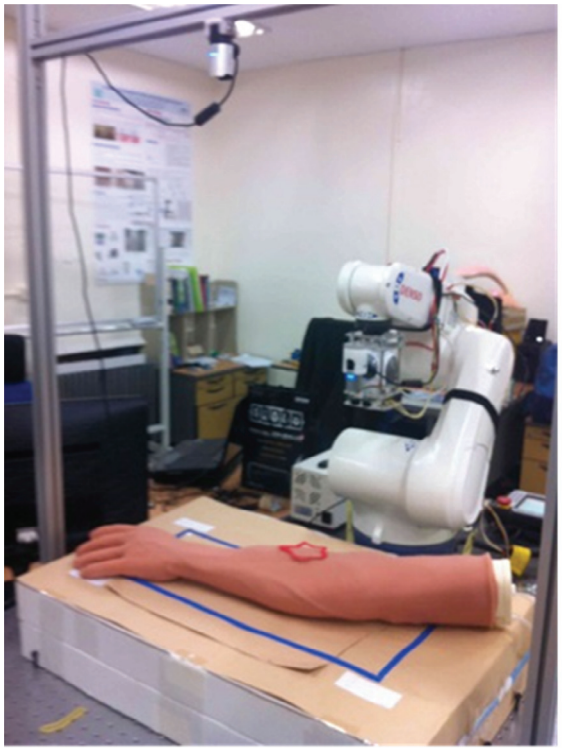

2 Webcams, a U/S sensor, and a Laser device as a set

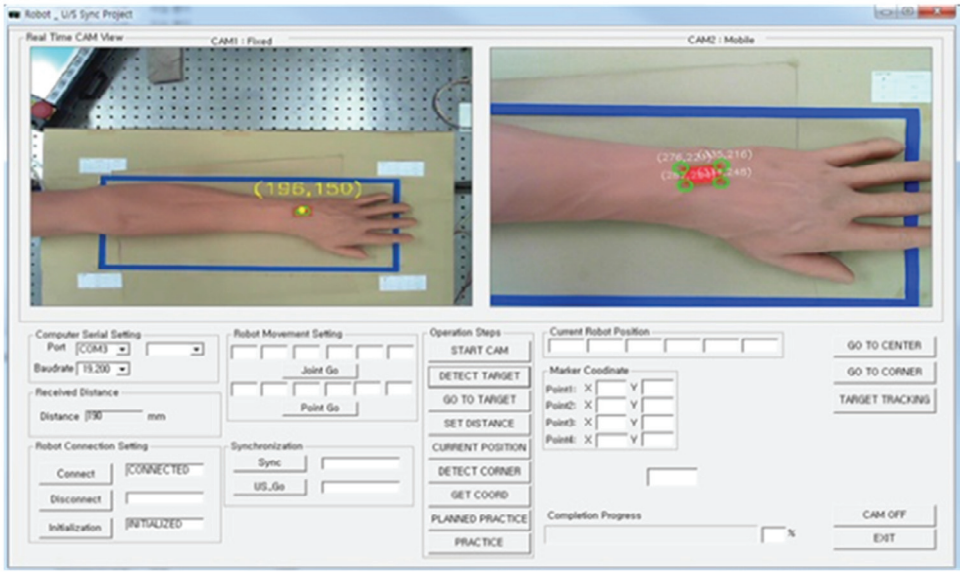

GUI Platform

Figure 2.3 Development of Version 0.8.

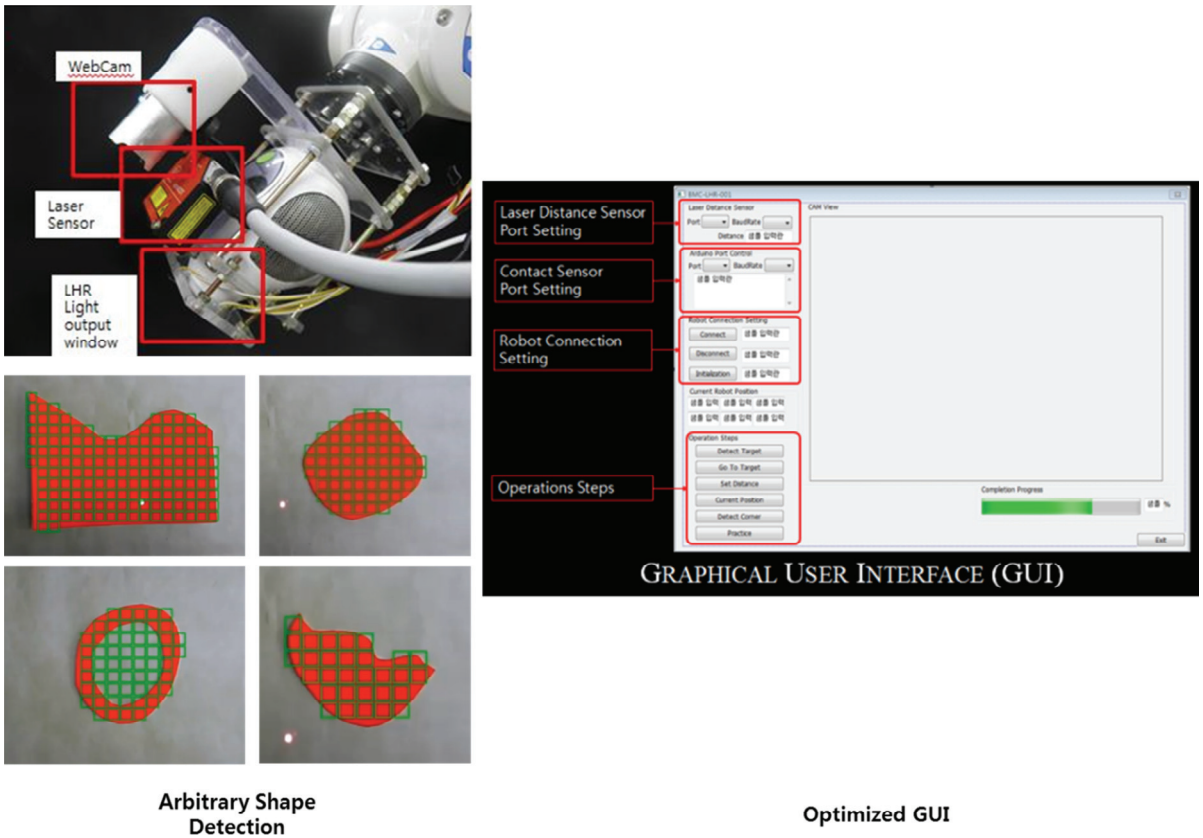

Figure 2.4 Development of Version 0.9.

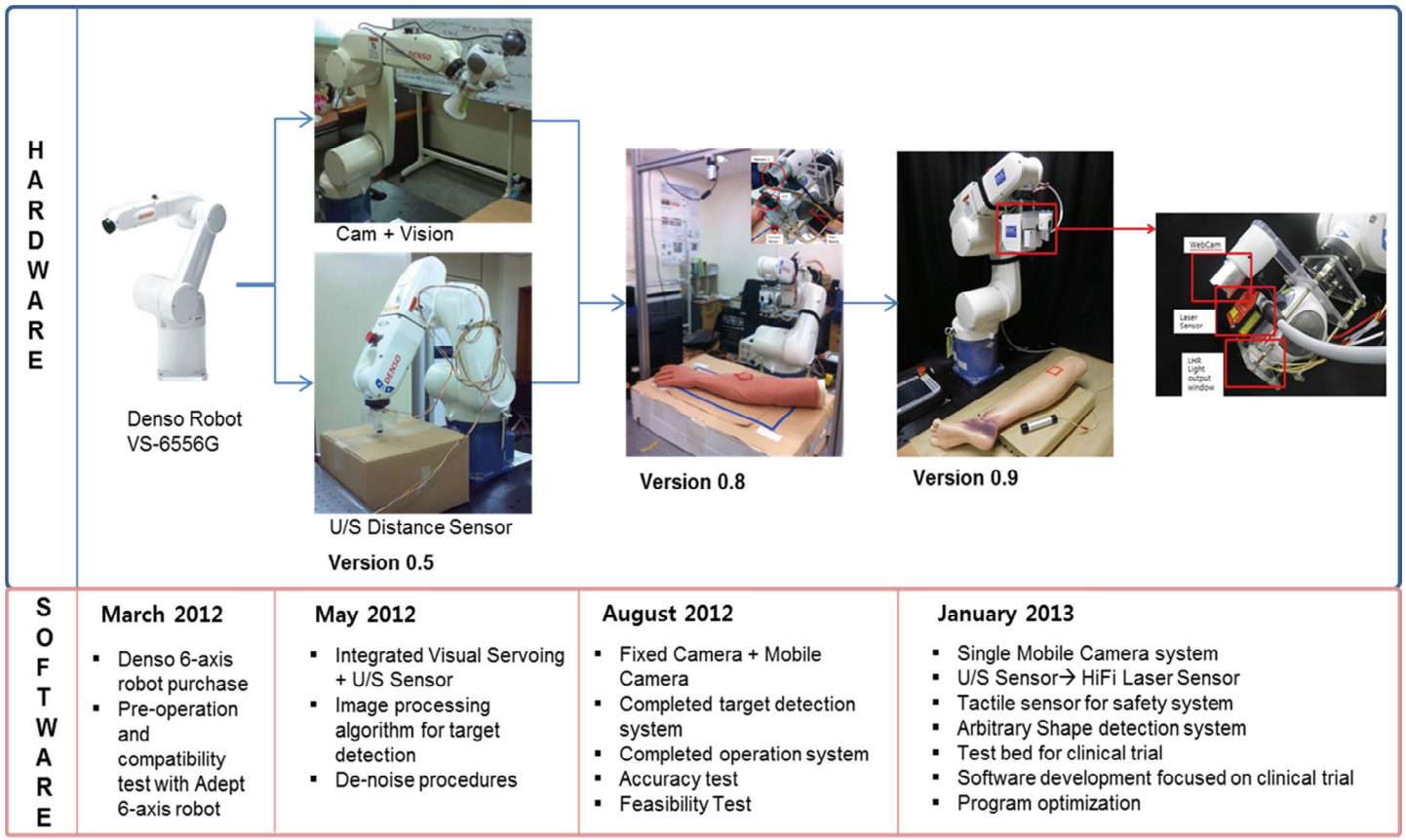

Figure 2.5 Brief history on the development of the system.

Fig. 2.8 shows the fixing structure that holds the camera, laser device, and laser distance sensor together. This structure fastens to the laser device with bolt and washer. The top part is attached to the robot's end with a M5 bolt.

The schematic of the system's case is depicted in Figure 2.9 and Figure 2.10 shows each component inside the case and the distance between each component. The end-piece case was designed using the Solidworks computer-aided design (CAD) program and printed as a product using a 3D printer. The material was polylactic acid PLA filament, and the case's thickness was 2 mm. The case was designed to protect the end-piece from physical impact and electrical shock from the environment. Figure 2.11 depicts a schematic of the workstation with its components, and Figure 2.12 shows an overview of the whole system.

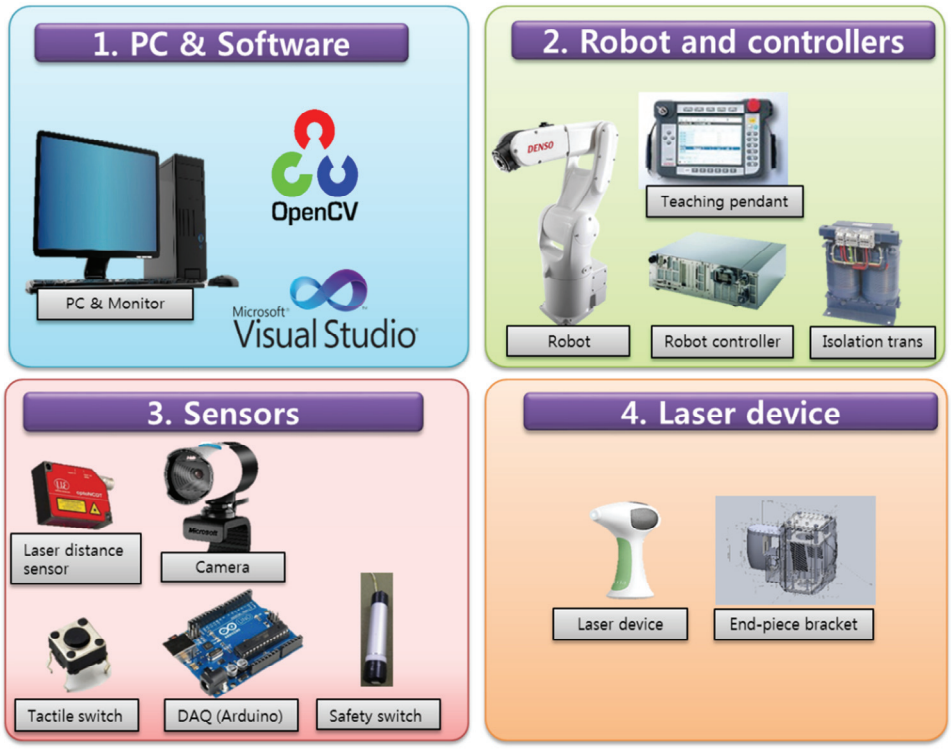

Figure 2.6 Hardware components of the robot-assisted automated laser treatment system version 1.0.

Table 2.1 Summary of the hardware device specifications.

Devices	Model, Manufacturer	Size (widthx length x height)	Others
LHR Device	Tria Plus, Tria Beauty	80 x 120 x 220 mm^3 (approx.)	Fluence:11−20 J/cm^2 Pulse Duration: 100−350 msec Wavelength: 810 nm
Laser Dist. Sensor	optoNCDT 1302, Micro−Epsilon	20 x 80 x 65 mm^3	Resolution Max: 4 μm
Camera	LifeCam Studio, Microsoft	40 x 113 x 50 mm^3	Autofocus, 1080p HD
6−axis Robot	VS−6556G, Denso Robotics	578 x 578 x 578 mm^3 (approx.)	Max Payload: 7kg Max Reach: 650 mm
Computer	Self−assembled	30 x 30 x 20 mm^3 (approx.)	Intel i7, 12Gb Ram
Sensor Controller	Arduino Uno R3, Arduino	53 x 75 x 13 mm^3	5V, GND, Programmable
Tactile Sensors	ITS−1109, Any Vendors	6 x 6 x 4 mm^3	Tactile sensor
Red paper target	Self−made	Arbitrary Shape	Red paper
Isolator	ES710/5000s, Bender	200 x 370 x 520 mm^3	Single phase transformer

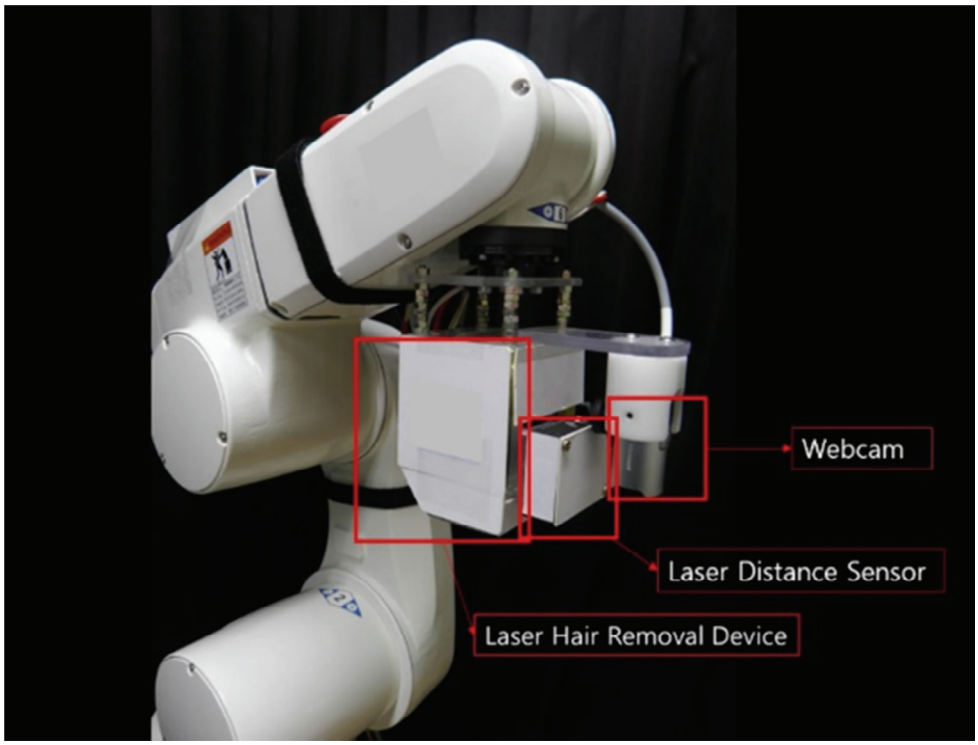

Figure 2.7 Proposed system's end-pieces attached at the end-effector of the 6-axis robot arm.

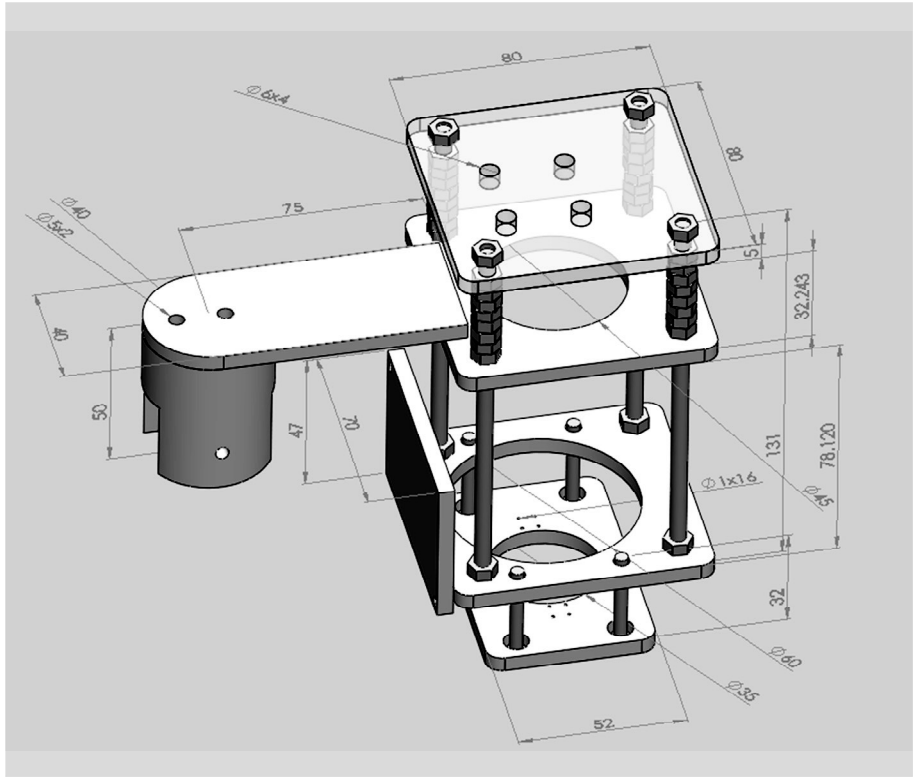

Figure 2.8 Fixing structure. The structure allows to rigidly fix the laser device, webcam, and laser distance sensor. Top is attached on the robot's end.

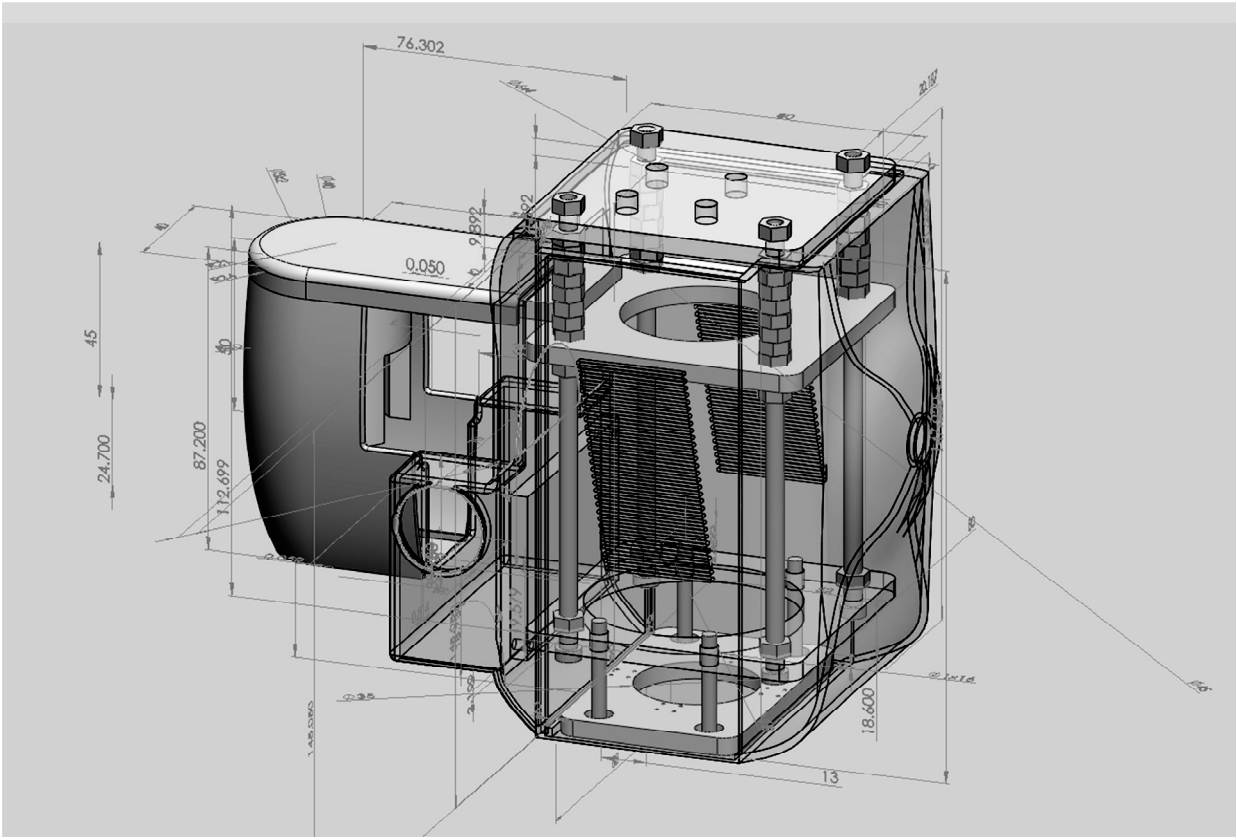

Figure 2.9 Version 1.0 end-piece's case. The case is the outer shell of the end-piece to cover the component.

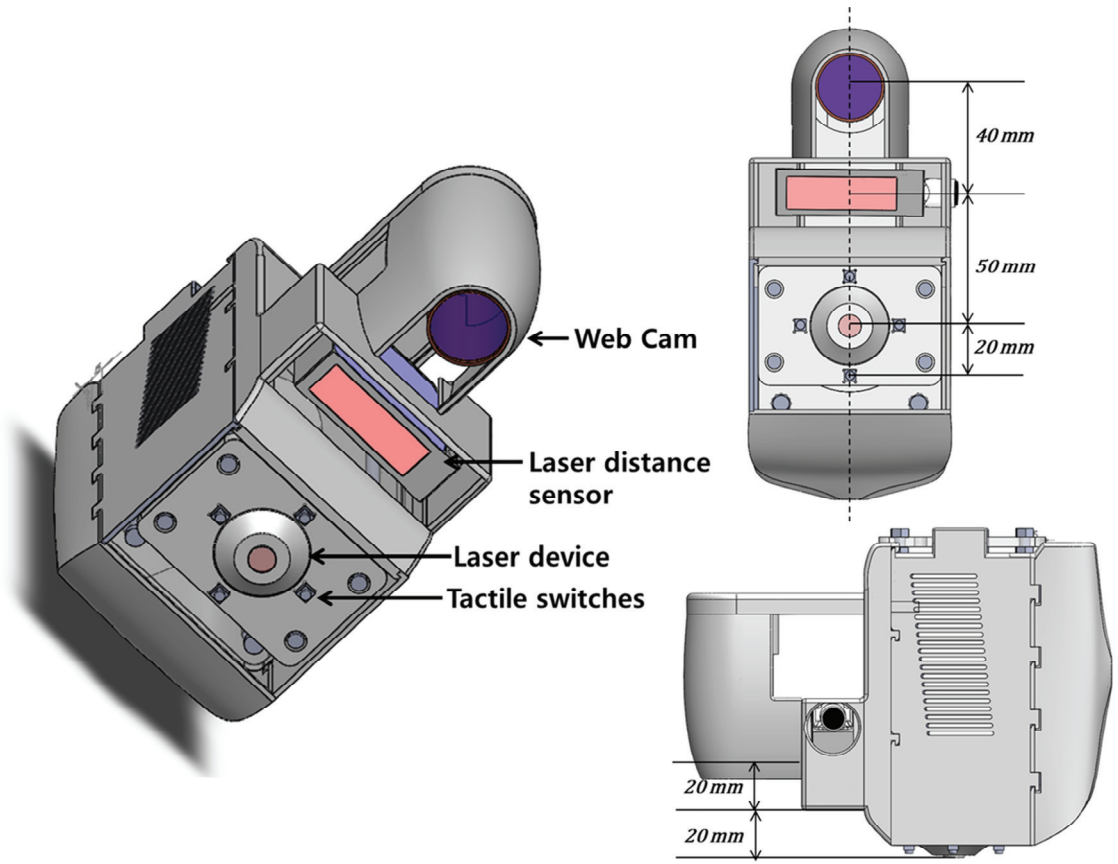

Figure 2.10 End-piece's case. Camera, laser dist. Sensor, laser device and tactile switches are installed and fixed inside the case.

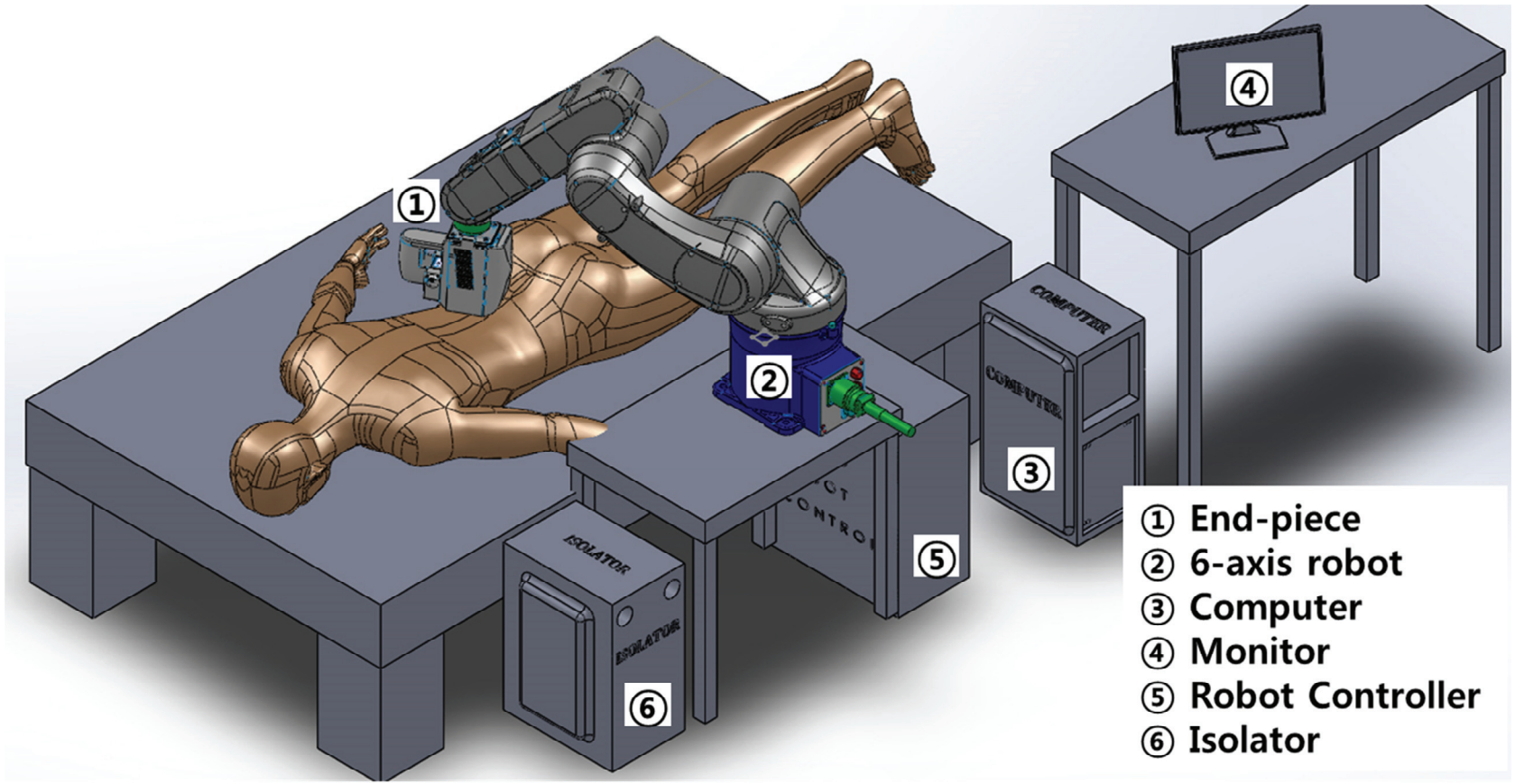

Figure 2.11 Schematic overview of the workstation.

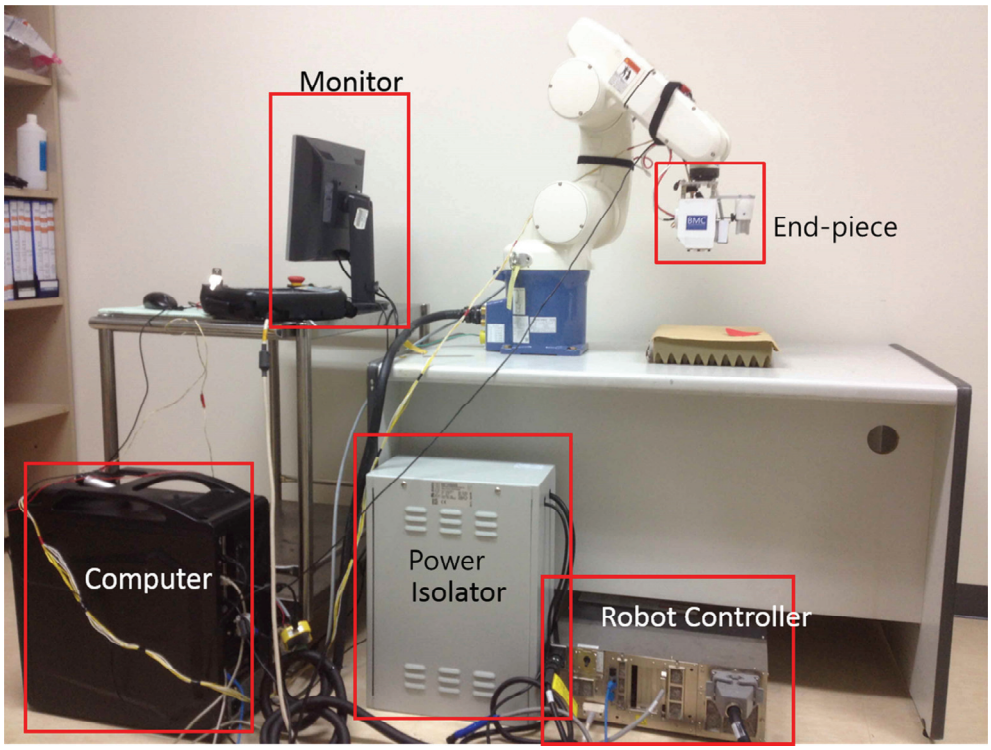

Figure 2.12 Overview of the entire system.

The laser device emits a laser pulse of 300 ms duration when three electrical sensors installed around the light output window (LOW) are simultaneously activated. The sensors receive the electrical signal and activate when the laser device contacts the skin. The sensors are installed around the circle with spacings of 120°, and each sensor is located 5 mm from the center of the LOW. Figure 2.13 depicts the skin contact sensors built inside the laser device, its locations, and the four tactile sensors built around the LOW.

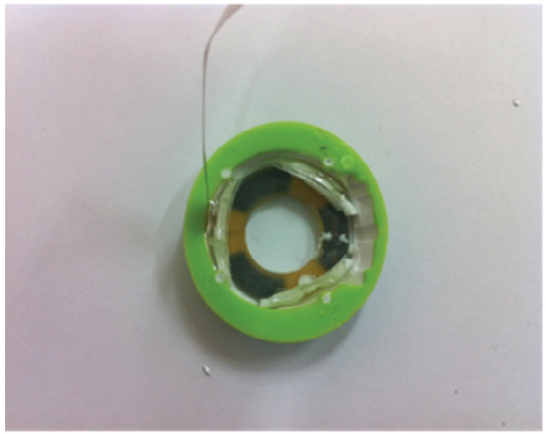

< Inside of LOW >

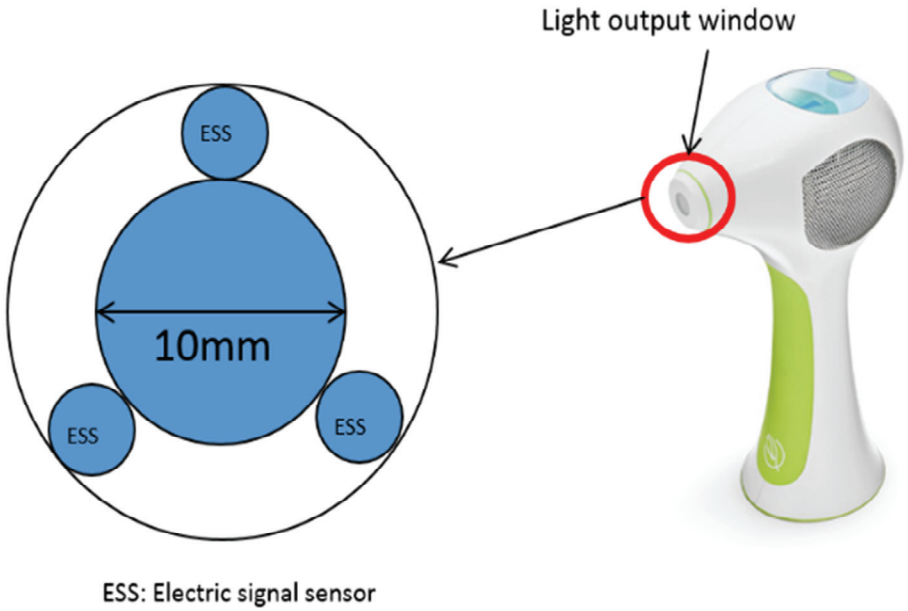

Figure 2.13 Skin contact sensors that are installed inside of LOW (light output window) and where it is located.

Four tactile sensors were attached to the plastic bracket in parallel with and alongside, the LOW as depicted in Figures 2.10 and 2.14. These tactile sensors function as a safety mechanism, which prevents unusually high and unnecessary pressure. If any one of the four tactile sensors is pressed and activated, the robot's end-effector returns to the initialization point and maintain the minimum safety clearance distance between the patient and laser device. The tactile sensor is activated when it is pressed with more than 0.49 N.

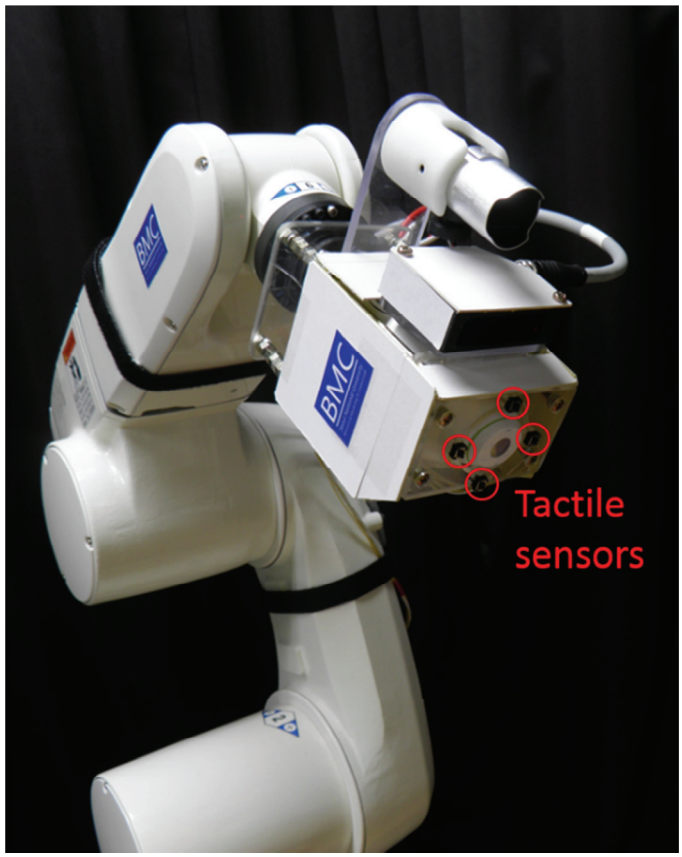

Figure 2.14 Tactile sensors built around LOW to prevent over-pressure.

An Arduino Uno R3 was used as a DAQ for the sensors, receiving 20 signals per second from each tactile sensor. The received data was sent to the computer via a universal serial bus (USB) cable, as shown in Figure 2.15, and thus integrated with the main operating system and shown on the GUI. Patients and physicians possess a stop switch and a robot control pendant, respectively, that they can use whenever they deem it necessary (Figure 2.16). When the switches are activated, the signal pauses the system, and the GUI provides a choice between resuming and aborting the work. The robot control pendant's stop button terminates every command, which stops the robot as soon as the button is pressed.

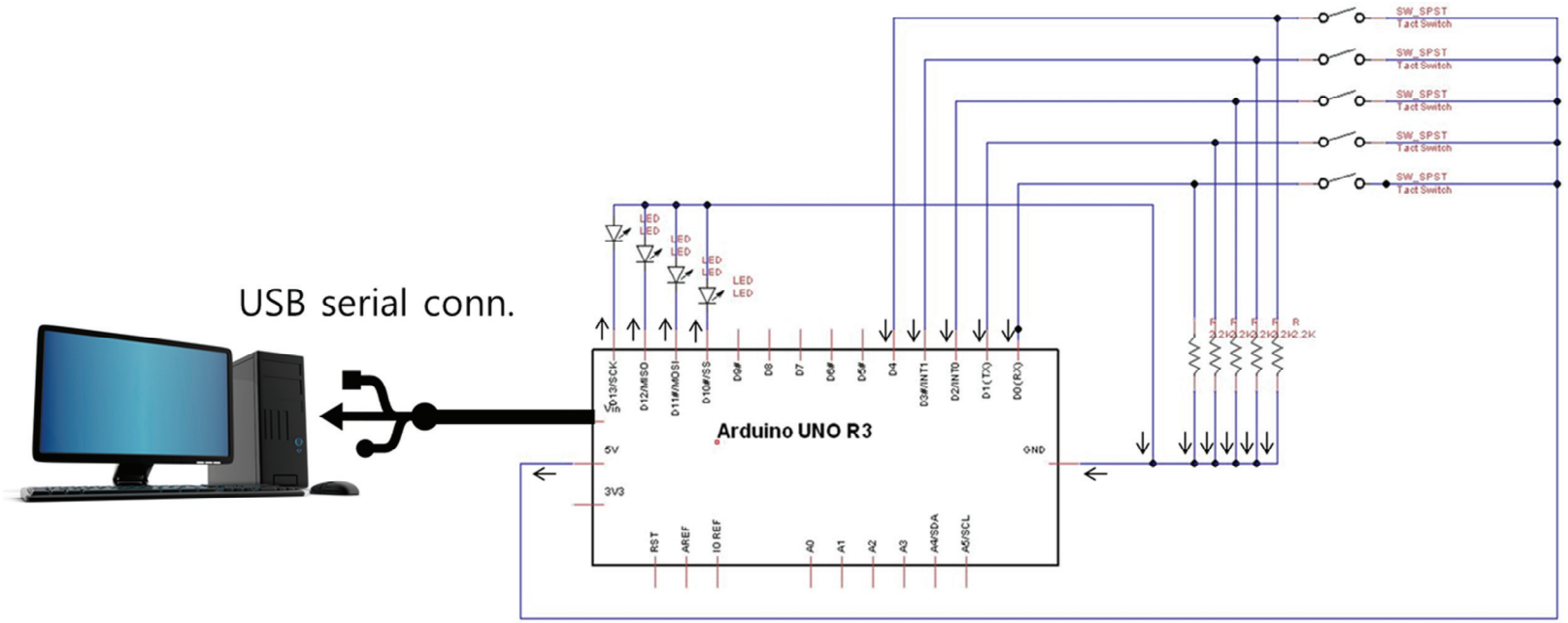

Figure 2.15 Schematics of tactile sensors connected to DAQ (Arduino UNO R3).

Figure 2.16 Stop switch for patient and robot control pendant for physician.

2.1.2. Software overview

For a robot arm to perform automatic laser irradiation, the system must receive accurate data of area and location of the target. To do so, image processing algorithm using edge detection method was adopted. The most intuitive and easiest method for physician to designate target area is to draw the perimeter of target which is the edge of the target or simply putting an arbitrary shape of red paper that has adequate size as a target on the patient's body. Image processing method using edge detection allows both methods to work.

In the present study, the target area to practice the "pick and place" motion is designated by red colored paper of arbitrary shape. The following describes the process how an object is recognized to be the target and how the coordinates are assigned.

The proposed system only recognizes the materials that are colored in red. This allows to easily differentiate the target object from the external environment. Moreover, it was experimentally figured that the color was less sensitive toward the change of surrounding light intensity.

To fulfill the goal of detecting target of interest, Microsoft Visual C++ Professional 2010 and OpenCV 2.4 were used as development software and image processing library, respectively. The list of

software specifications is provided on Table 2.2

The proposed system uses the "pick and place" technique, due to its flexibility in application, as well as confirmation of the laser-irradiated spot and the spot to be irradiated. It is assumed that the region of interest (ROI) for the laser irradiation target is a smoothly contoured surface area, in which no rapid rise or fall exists. The target was considered to be immobile. The difference in height from one spot to another is assumed to be small and the workspace area is less than 200 x 400 mm^2. The camera (LifeCam Studio, Microsoft, CA) attached onto the end-piece automatically detects any arbitrarily shaped and sized target in red. Then, the robot executes the "pick and place" motion on the target's entire area. Figure 2.17 shows the software algorithm order of the proposed system. The laser is irradiated only when its laser output window (LOW) is in full contact with the skin, for maximal efficacy and safety.

Table 2.2 Summary of the software specifications.

Software	Manufacturer	Role
Visual Studio MFC 2010	Microsoft	Integrated development environment (IDE)
MEDAQLib V3.2.1	Micro-Epsilon	Laser distance sensor control program
OpenCV 2.4.2	Intel	Vision and image processing library
Arduino 1.0 IDE	Arduino	Arduino signal processing control program

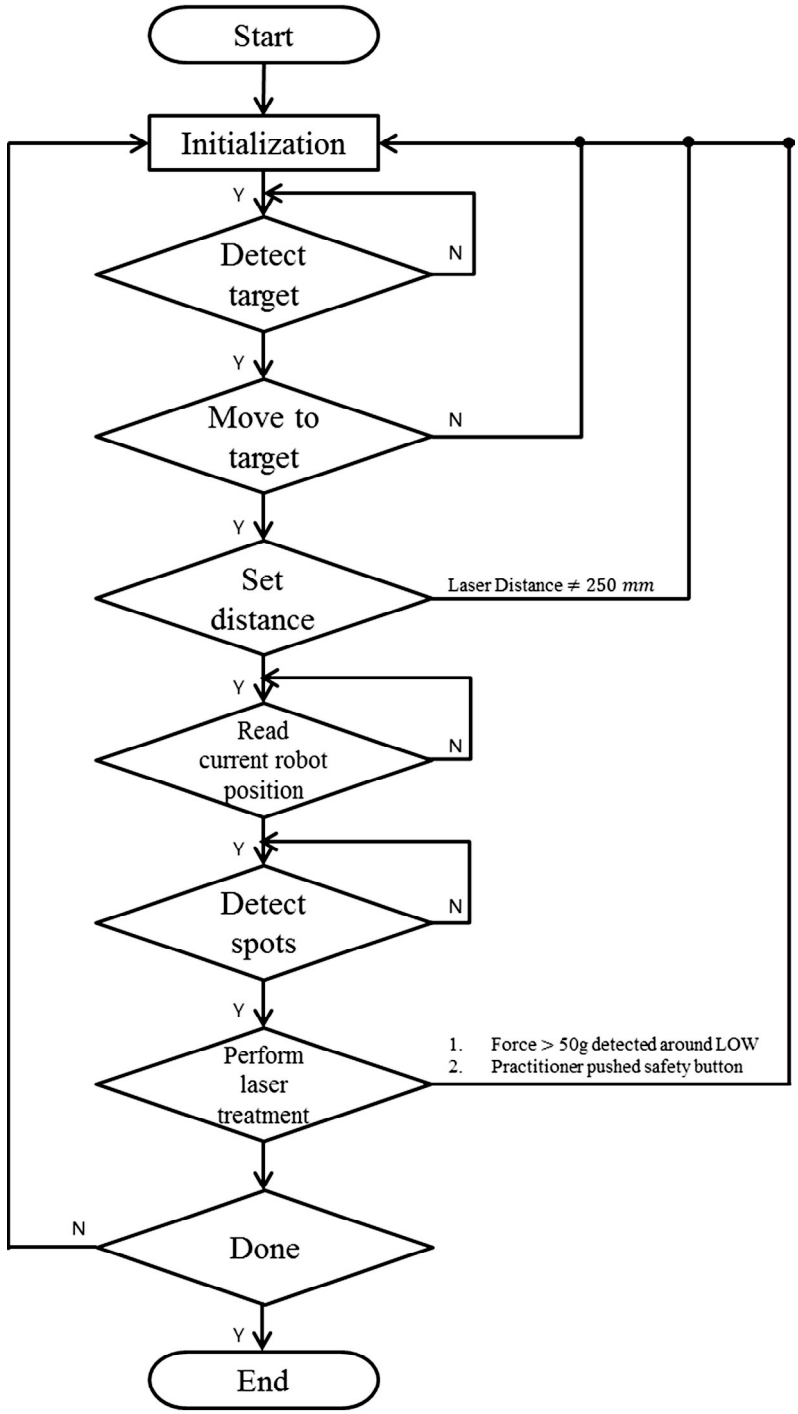

Figure 2.17 Software operation order of the system (Details are shown in Figure 2.18).

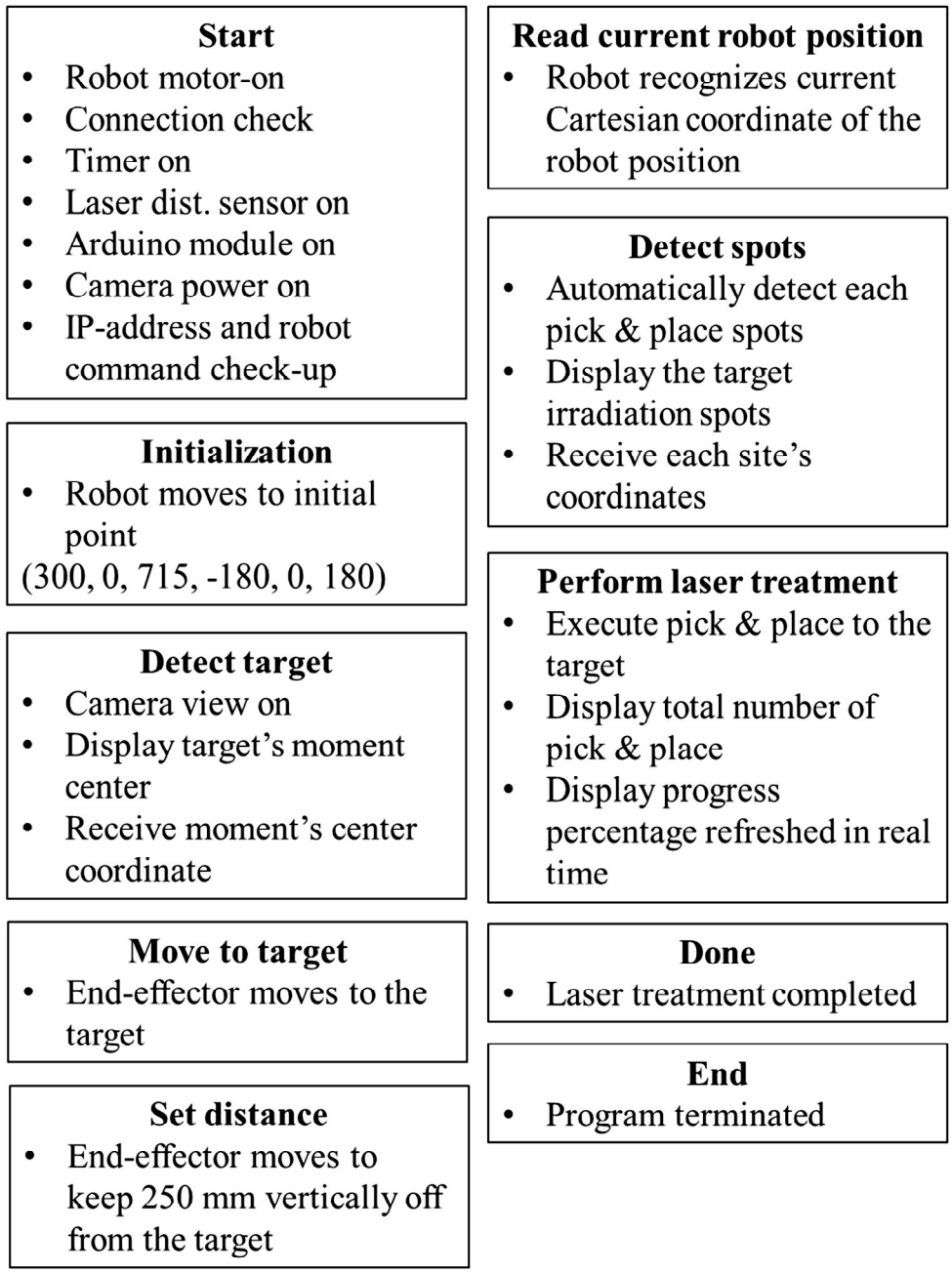

Figure 2.18 Explanations of software order of the system.

Figure 2.18 explains the functions activated on each block diagram. The “connect” step connects robot controller, camera, laser distance sensor, Arduino DAQ with computer. Robot controller is connected with local area network (LAN) therefore, proper IP address has to be set between the controller and computer. Camera, laser distance sensor, and Arduino DAQ is connected through serial USB cable to pc. After these components are connected, the robot’s motor, laser distance sensor, Arduino DAQ module, and webcam gets activated. The “Initialization” step makes robot to move to a specific location where safety distance between the robot’s end-effector and target. It mostly function as initial starting point and come-back point when the tactile switch is activated. The “Detect Target” function is literally detecting the target. The system automatically detects the red target within its view. Its coordinate data of moment is numerically shown on the monitor and the operator can check the status whether the system detected the target correctly or not. “Go to Target” enables the robot’s end-effector to move to the target. “Set distance” is an important step because the calibrated measurement is set up and saved on the distance of 250 mm between the object and the camera. Robot is programmed to keep this distance before “Detect Corners” step so the robot can perform laser delivery regardless of the target’s location. “Practice” step executes pick & place motion on the target and starts to deliver the laser in uniform distribution.

Figure 2.19 shows the image processing algorithm for target detection followed by 'labeling' and Figure 2.20 depicts the results of each important image processing steps. Once the system receives the raw image from the camera, the system undergoes color segmentation. The red−green−blue (RGB) color segmentation is used to isolate the object of a specified color range in an RGB image[24]. Using this method, we have made condition to select the color channel of red. As a next step, median filtering of 3 x 3 pixel was used to reduce the noise of the image.

Up to previous point, we have made the image ready for edge detection. Canny edge algorithm[25] assembles the individual edge candidate pixels to contours so that two thresholds, an upper and a lower one, are formed. Only the edges within two threshold values are accepted[26]. The present system used 8−bit gray scale binary threshold, in which any pixel values > 90 are converted to 255 (white), and values < 90 are converted to zero (black). The edge detection displays the boundary of the target. Next step is to figure out the location, area, shape of the target through image analysis.

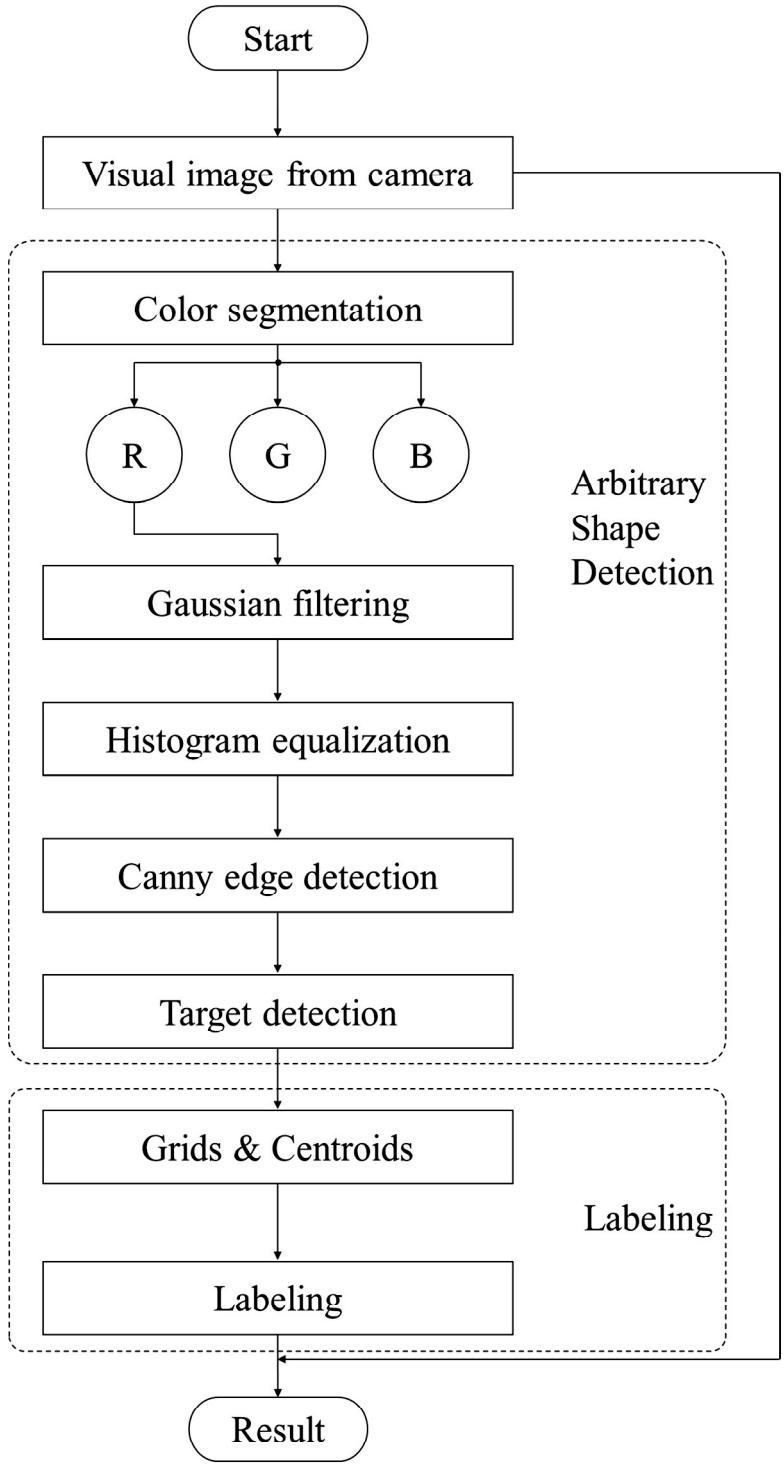

Figure 2.19 Image processing algorithm for arbitrary shaped detection and labeling.

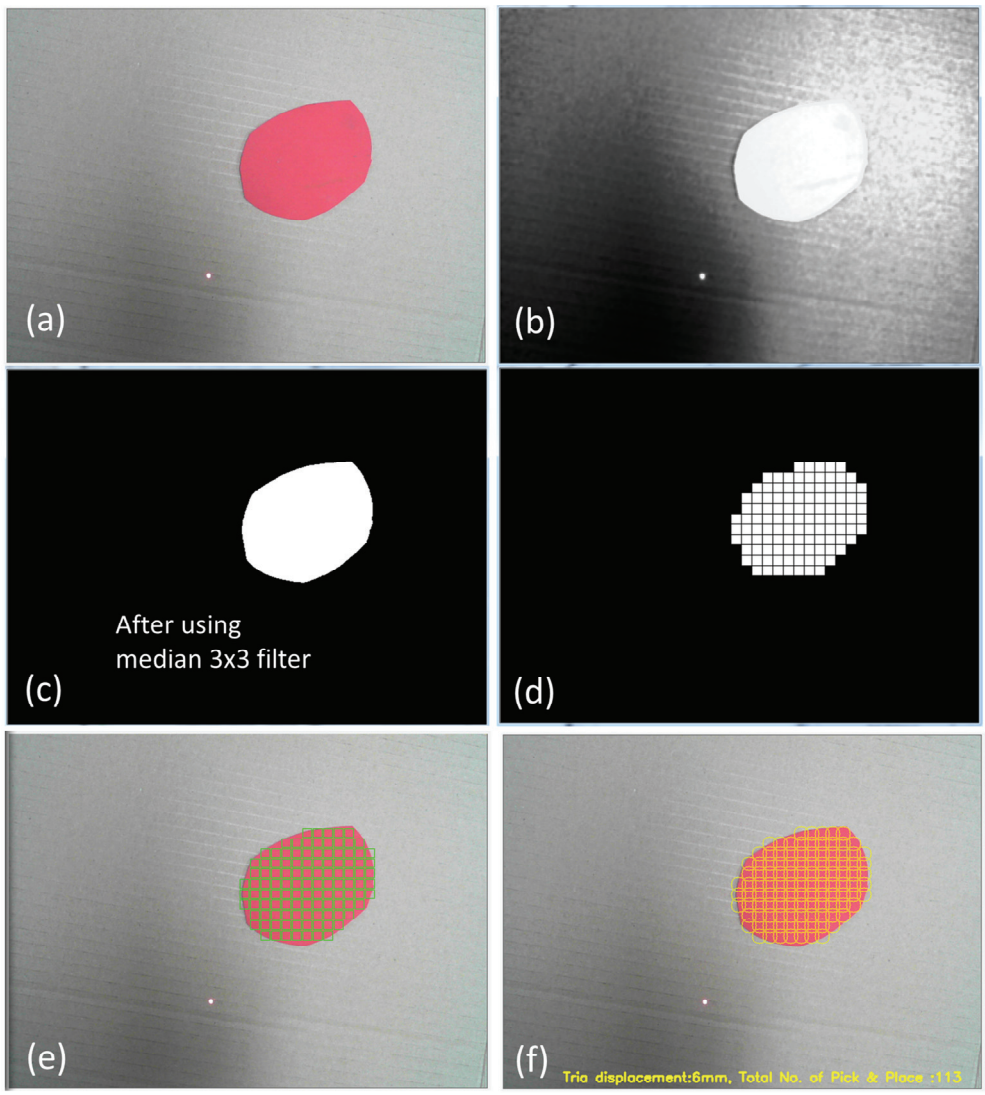

Figure 2.20 Sequence of image processing steps from original image to grid patterns. (a) Visual image from camera, (b) after channel selection and Gaussian filtering (c) after histogram equalization, median filtering, and canny edge detection (d) after target detection and grids patterning (e) after labeling (f) locations of laser irradiation.

To detect the center of the arbitrary target, the concept of the geometric centroid is adopted. Image moment is a certain particular weighted average of the image pixels' intensities. Area, its centroid, and information about its orientation can be interpreted through moments. The greyscale image with pixel intensity,$I(x,y)$, the image moment $M_{i,j}$ are calculated by

$$M_{i,j} = \sum_x \sum_y x^i y^j I(x,y) \ where\ x,y \in R \tag{2.1}$$

According to the above equation, the coordinates of the centroid $(\bar{x},\bar{y})$ are

$$\bar{x} = \frac{M_{1,0}}{M_{0,0}} \quad \bar{y} = \frac{M_{0,1}}{M_{0,0}} \tag{2.2}$$

$$sum_x = \sum\sum xI(x,y) \quad \text{and } I(x,y) = 1 \tag{2.3}$$

$$sum_y = \sum\sum yI(x,y) \quad \text{and } I(x,y) = 1 \tag{2.4}$$

$$M_{1,0} = \frac{sum_x}{M_{0,0}} \quad M_{0,1} = \frac{sum_y}{M_{0,0}} \tag{2.5}$$

where $M_{0,0}$ is denoted for the area of the arbitrary target. $M_{1,0}$ and $M_{0,1}$ can be extracted with following method and equation 2.3 and

2.4. The two summations denoted in equation 2.3 are like a for loop. The x coordinate of all white pixels (where I(x,y)=1) is added up. It operates similarly for equation 2.4. The robot will move to this coordinate and maintain a distance of 250 mm from the target by measuring through the laser distance sensor. The center of the camera's image frame is matched with target's center coordinate.

In order to implement 'pick and place' movement, gridlines were made on the image of the target and coordinates of each grid's center were saved as an array and were designated as coordinates where robot will irradiate laser pulse. Figure 2.21 depicts the grid patterns of the laser delivery. The system allows to setup the distance between a shot to its next shot because it should be depend upon the size of the LOW (light output window). Bigger LOW will have longer distance from one shot to its next. The diameter of the LOW was 10 mm which make $10/\sqrt{2}$ (7.1) mm to be the idealistic distance between shots. We have assumed the clinically effective area will be less than the size of output window. Since the energy distribution from the laser output follows Gaussian distribution form which makes the energy to be drastically reduced as the distance from the center increases, the distance was setup as 6 mm. It was also a suggested distance from manufacturer's recommendation as well. As a last step, the coordinate data of grid were saved in numbered order using blob labeling. Each spots were

given numbers and their x and y coordinate data were labeled and saved in the matrices. This allowed numbering each grid; always the grid on left top to be the first while right bottom to be the last. Arbitrary shape is not a standardized shape by any mean, therefore, edges are not always straight lines either. However, LOW will always be either a rectangle or a circle which is a standardized form. The shape of LOW was a circle with 10 mm diameter which not always fit inside of the edge. In this case, if the grid was filled more than 60% the grid was counted while less than 60 % was discarded.

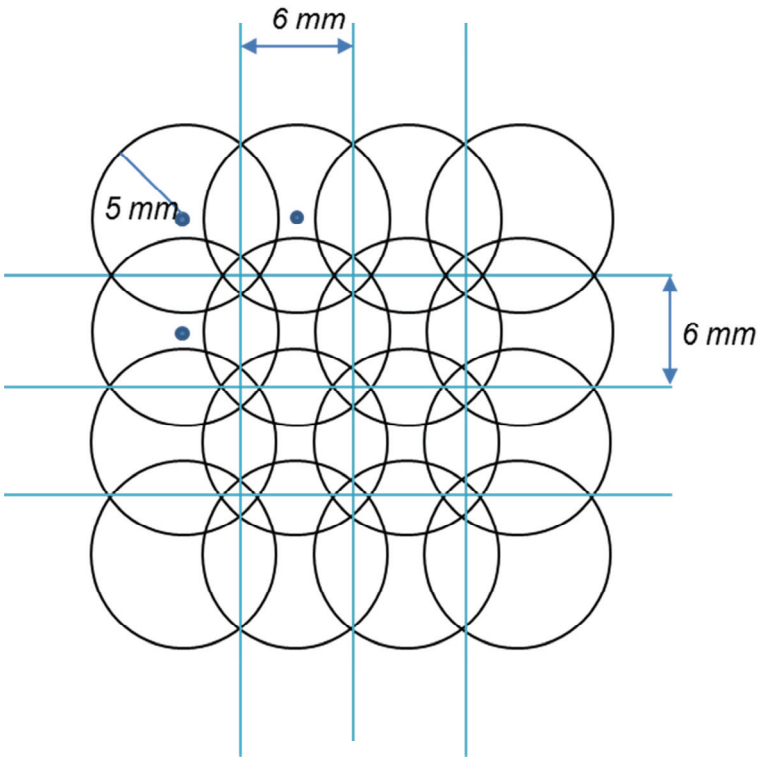

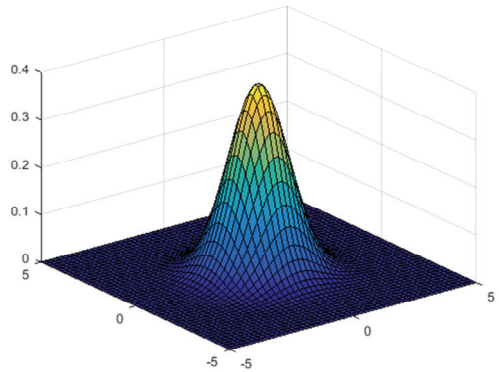

(b)

Figure 2.21 (a) Laser output window size, grid size, and distance between each neighboring spot (b) laser intensity shown in Gaussian distribution model (Normal distribution).

Figure 2.22 illustrates the target's edge detection, centroid, grid lines and labeling, and pick and place motion. The main function of GUI is to show the information of expected target area of laser delivery and operation steps to patient and physician. It also displays the completion progress bar and completion percentages. The 'Detect Target' button located on bottom left of the GUI allows to immediately detect edge lines and centroid as shown on Figure 2.22 (a). When the 'Detect Corner' button is clicked, it shows the grid on the target and locations of where the laser will be irradiated as shown on Fig. 2.22 (b). Once the 'Practice' button is clicked (Figure 2.23), the 'pick and place' motion is performed on the grids. The black circles are where it was irradiated while yellow hollow circles are where it has not been delivered yet but will be. Along with visual information, quantitative information such as displacement distance, total number of irradiation, completion progress bar and percentages are confirmed through GUI.

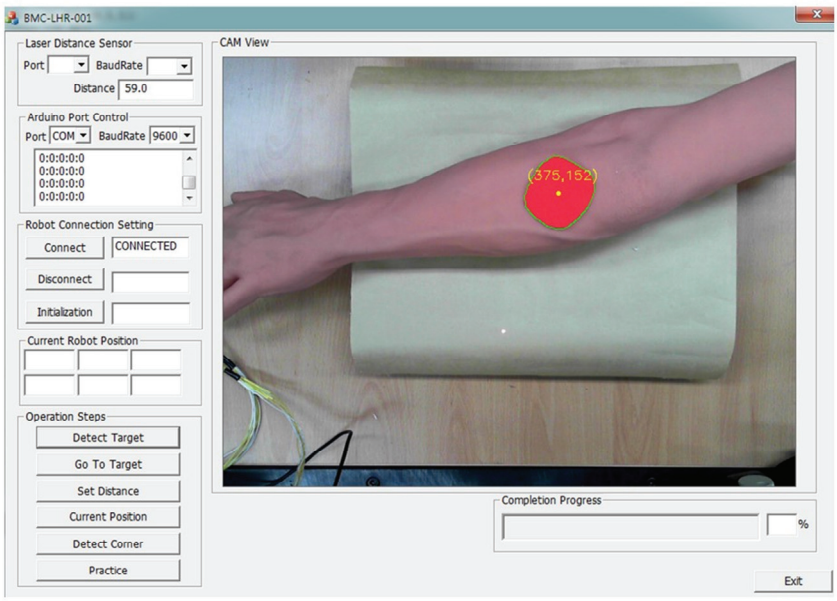

(a)

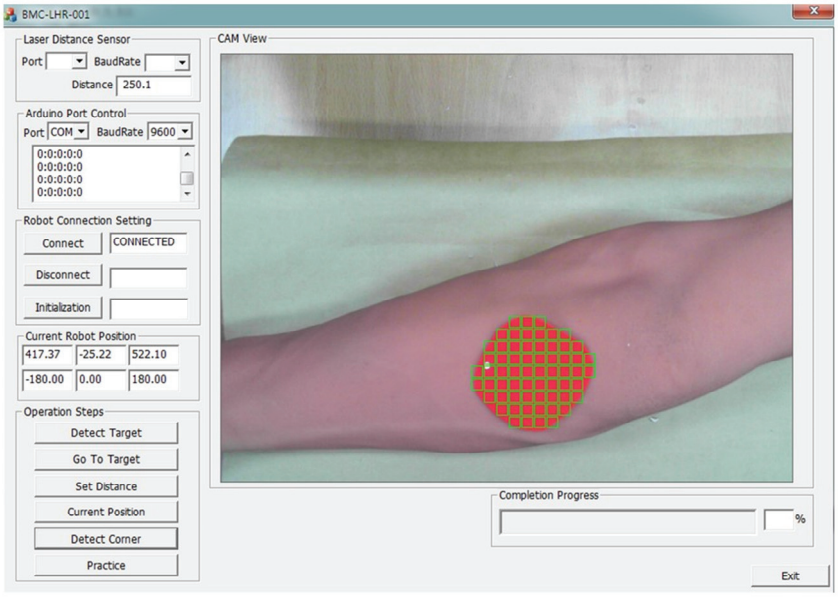

(b)

Figure 2.22 Steps of operations results. (a) Target is detected (b) grids and each of its locations.

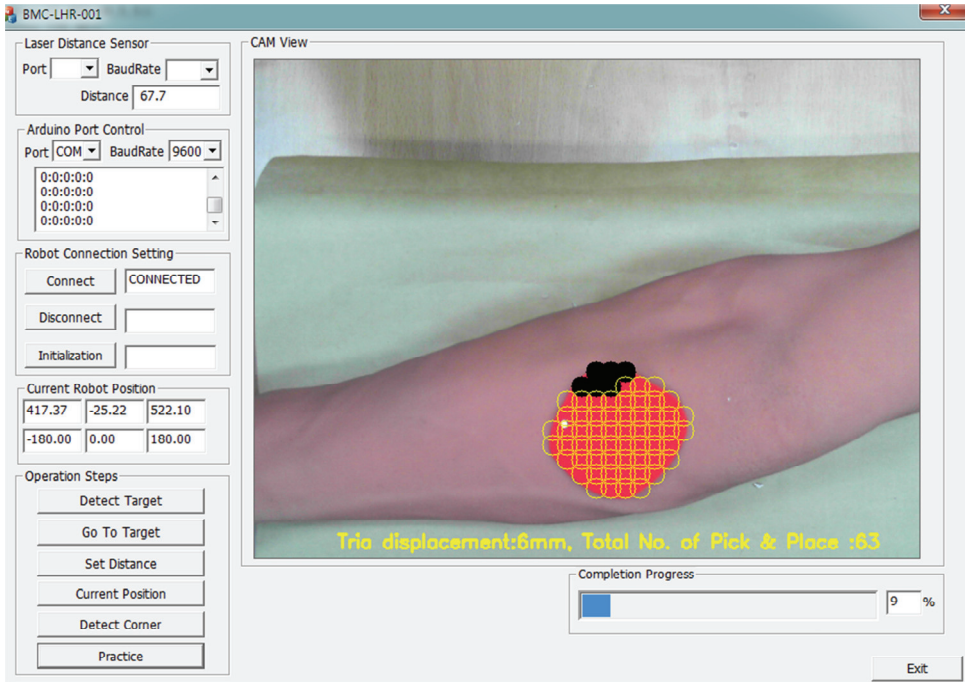

Figure 2.23 Image during the practice of the system

2.1.3. Sensors and coordinate system

The target's 2D planar information can be figured through camera but the information on depth is required in order to successfully irradiate laser on the target which can be anywhere in terms of 3 dimensional space within the camera view. There are several methods that can be used to collect 3D coordinate data. Stereo vision, laser 3D scanner, three 1-dimesional distance sensor used at once, 6-axis force-torque sensor, ultrasound distance sensor, and finally the 2D camera vision system with the 1-dimensional laser distance sensor. During the primitive stage of the development, ultrasound sensor was used to measure the distance between object and the sensor. It was low-cost, light weight, low-power, and fulfilled its purpose under the assumption of 2D space where no rapid rise and fall of curvature exists. However, the ultrasound sensor module we were using (HG-C40U, Hagisonic, Korea) had critical deficit on measuring distance when measuring on human body surface. The Doppler effect, which is basic principle of measurement method, searches the shortest distance between object and sensor within the beam-spread angle (65°) as shown in Figure 2.24. The distance cannot provide accuracy nor reliability if used during the clinical trial. Therefore, it was replaced with Hi-Fi 1-dimensional laser distance sensor

(OptoNCDT1302, Micro-epsilon, Germany).

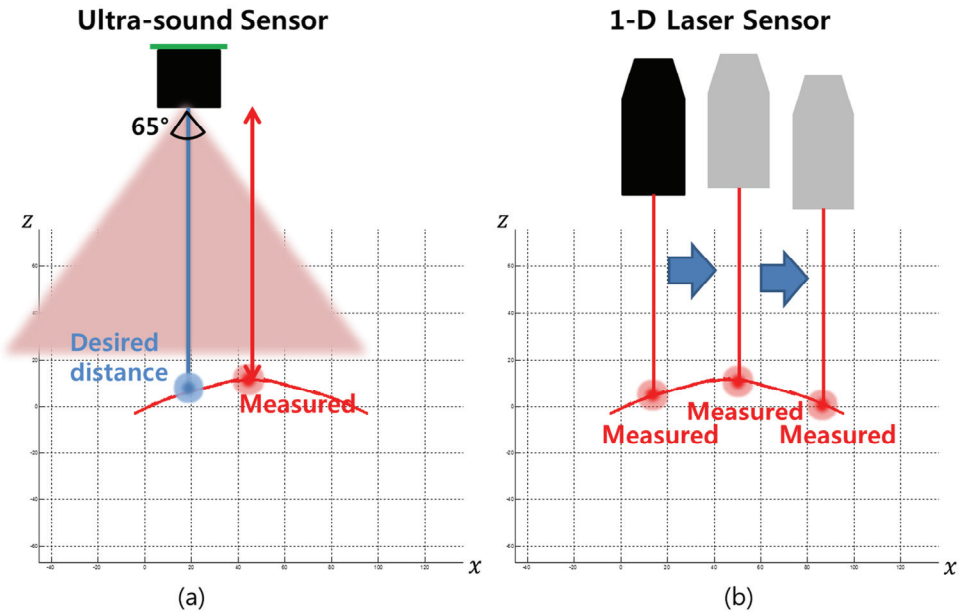

Figure 2.24 Difference between the (a) Ultra-sound sensor and (b) 1-D laser sensor

The proposed system required accuracy and precision along with fast readiness since it is designed as a medical device that has to be ready for clinical trial. Choosing the right combination of sensors were very important since accurate data received directly affected accurate robot coordinate and robot movement. Stereo vision does not provide accurate (within millimeter or less scale) depth data nor is it reliable to handle real time image processing. Laser 3D scanners do provide accurate 3D coordinate (x, y, and z)

information of the target's surface but it cannot readily respond for clinical use. Therefore, considering all the pros and cons of the sensors, we chose 2D camera vision system with the 1-dimensional laser distance sensor. We used 1-dementsional laser distance sensor for its micro level accuracy, low power laser beam irradiation (< 1 mW), physical appearance of laser beam spot right on the surface of the target.

Figure 2.25 (a) shows the coordinates of the objects relative to the camera coordinate frame. The coordinates C^x and C^y form the image plane, which is parallel to the horizontal axis of the image while aligned with the optical axis of the lens. The end-piece coordinates are denoted as R^x, R^y, R^z, which represent the Cartesian coordinates x, y, and z, respectively. The end-piece is the device at the end of the robot arm. In this study, a unit composed of laser device, camera, tactile sensors and laser distance sensor is the end-piece. Figure 2.25 (b) shows the simplified application of the proposed system operating on a human back. The position of the six axis robot arm end-effector is expressed in terms of the reference frame, which is the robot base, denoted as O^x, O^y, O^z. Overall, the position of the camera and laser sensor are fixed within and by end-piece' s skeletal structure and both remain perpendicular to the base ground.

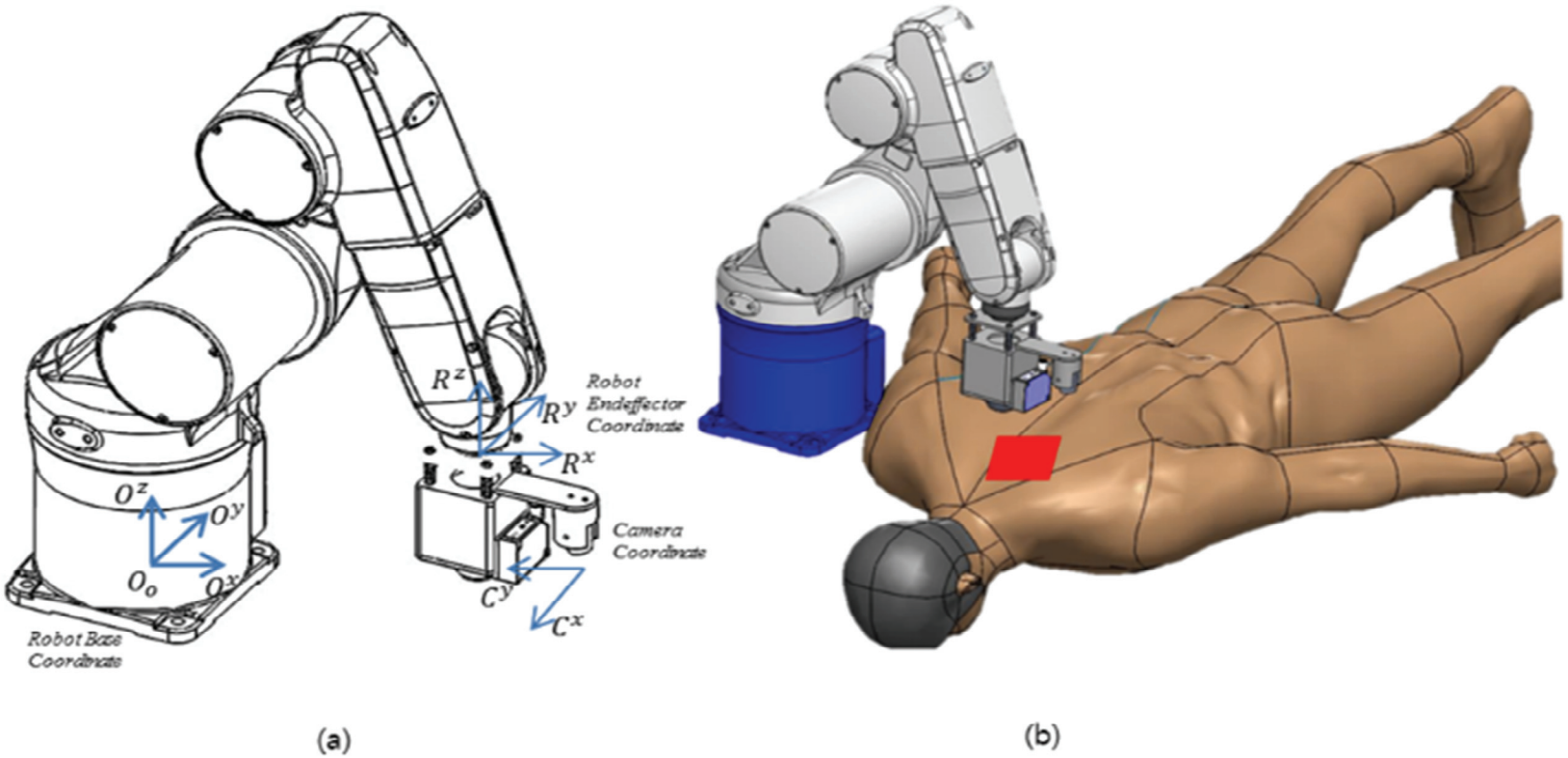

Figure 2.25 (a) robot base coordinate, end effector's coordinate, and camera coordinate. (b) virtual patient in treatment.

By using the one-dimensional laser distance sensor, the distance between the sensor and the object can be received. The laser sensor continuously projects a laser-generated red dot on the object's surface for visual location. Also, a z-coordinate value for robot can be easily obtained, because the end effector is controlled to be parallel to the base ground throughout the procedure.

As introduced from the previous section the virtual gridlines are generated on the image, using both horizontal and vertical lines, such that each grid's center coordinates are 6 mm apart from its neighboring grids. Using the gridlines, we determined the designated locations for the assigned "pick and place" coordinates of the arbitrarily shaped target.

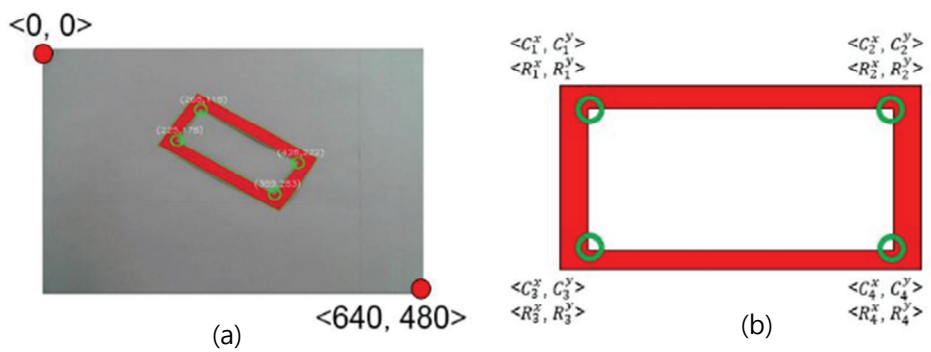

Figure 2.26 Coordinate mapping example. (a) Coordinates received from the camera, (b) parameters of each coordinate used for mapping.

After each of the desired coordinates for "pick and place" is extracted, the robot's end piece moves toward each location of the target. While the camera's visual data are used to collect the planar location, the laser distance sensor is used to calculate depth. The laser sensor, which is fixed at the end effector, measures the precise distance between the target and the laser sensor, and then the data are used for robot control, to enable contact with the target. The basic mechanism involves mapping (coordinate transformation) the extracted camera coordinate to the robot's coordinates. The following equations 2.6 & 2.7 and Figure 2.26 describes the method for mapping, how camera coordinate is transformed into robot's coordinate and equation 2.8 is used to maintain the 250 mm vertical distance from the object.

$$R_x = \frac{R_3^x - R_1^x}{C_3^y - C_1^y} C_y + R_1^x - \frac{R_3^x - R_1^x}{C_3^y - C_1^y} C_1^y \tag{2.6}$$

$$R_y = \frac{R_2^y - R_1^y}{C_2^x - C_1^x} C_x + R_1^y - \frac{R_2^y - R_1^y}{C_2^x - C_1^x} C_1^x \tag{2.7}$$

Where R_x and R_y are the end effector's x and y coordinates, respectively, and C_x and C_y, are the camera's x and y coordinates, respectively. The R_n^x and R_n^y are the end-effector's coordinate values extracted from corresponding camera coordinates C_n^x and C_n^y.

Since the laser distance sensor produces continuous beam spot and it is always directed perpendicular to the ground, therefore, R_n^x and R_n^y can be extracted from the robot's encoder value when the laser beam spot is located on the expected location. The camera coordinate values are measured in whole number, while those of the robot are returned with a precision in the hundredths decimal.

$$Z_d = Z_{Cur} - (Z_l - Z_r) \tag{2.8}$$

where Z_d, Z_{Cur}, Z_l, and Z_r are the desired $z-$coordinate of end-effector, the current $z-$coordinate of the end-effector, the measured value from the laser sensor, and the reference distance which is 250 mm, respectively.

2.1.4. Markers

The markers are used to detect the area of treatment. The size and shape of the marker will be designated as the area and locations where the treatment will be conducted. The marker can be either filled or hollow. There are two way to designate the area of laser delivery. One is to cut the non-reflective red colored paper as one desires and put it on top of patient's body where laser treatment shall be delivered or simply just draw the boundary of desired laser delivery site with red paint on the patient's body. When drawing the boundary, it has to be a closed loop. Otherwise, the system would not recognize as area to be irradiated. Any shape less than 18 x 22 cm^2 is allowed per trial. The red color is chosen for following reasons. First, the detection algorithm is governed by colors for it facilitates the noise filtering. The red color itself is an unusual color and it also has its own channel in RBC color parameter which makes it distinguished compared to other colors. Using homogeneous colored material is preferred for noise filtration. Color method also provides the direct visual cues to practitioner since it can be drawn on the body of patient. It give confidence to practitioner where the laser will be delivered. Method for detecting arbitrary shape through image processing is explained on the next section, the image processing method.

2.1.5. System verifications

Localization–error test

The localization error test was used to validate the accuracy and precision of the automated proposed system was assessed by comparing the detected target' s position with the reference coordinates of the robot. The graph paper is precisely positioned in accordance with the robot' s reference coordinate point, p_{ref}^{tgt}, which serves as a reference to be measured (Figure 2.27). The dimension of the test area is set to 400 x 200 mm^2, which is sufficient to cover a human back; the 15 points with an equal distance of 100 mm from each neighboring point are depicted in Figure 2.27. A 6 x 6 mm^2 square red colored paper target is placed on points ranging from P^{11} to P^{35}. The target' s position is well placed on the graph paper to minimize the displacement error by carefully matching its center with the reference point. Because the laser distance sensor is fixed within the robot' s end–piece, the laser beam is always pointing perpendicular to the ground, which serves as a visual locator. The proposed test is to simply detect the 6 x 6 mm^2 red colored paper target and to move to the target from the initial position so that the laser distance sensor' s laser beam is reflected on the target. Because the robot' s encoder provides the Cartesian coordinate values of the end–effector' s position, it is utilized to test the localization capability of the proposed system. A

round of the test set consisted of moving P_{11} to P_{35} without staying more than once per position, which is manually moved from each point, and 10 rounds of the test are performed to provide 150 samples of data.

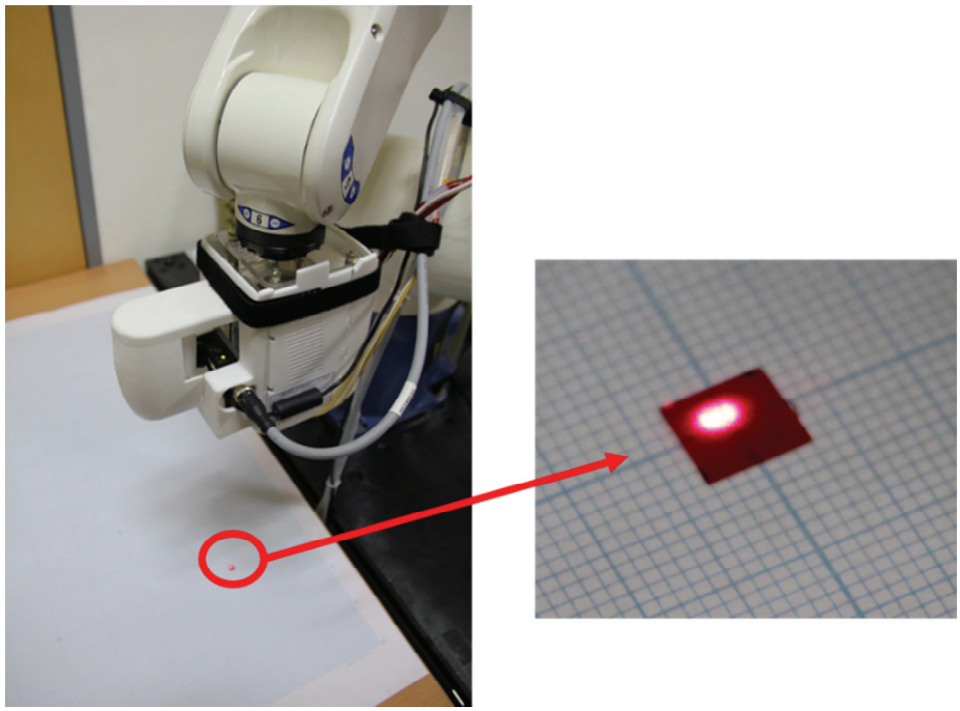

Figure 2.27 Localization test performed on the graph paper. The red luminescent dot is the laser beam from the laser distance sensor while red square is the 6 x 6 mm^2 marker.

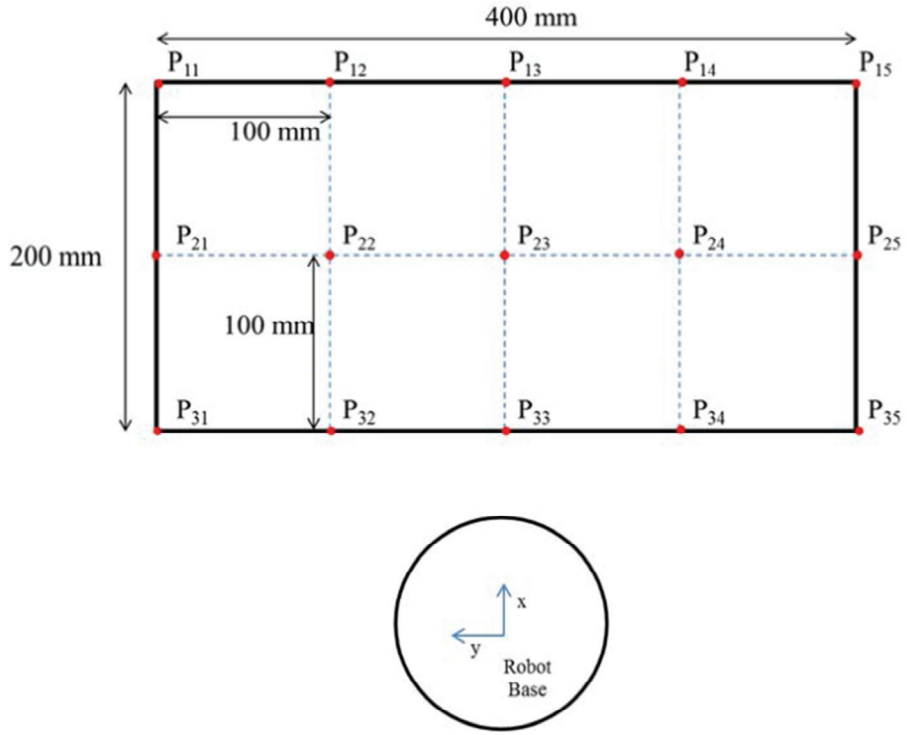

Figure 2.28 Localization test board on graph paper. Total dimensions in 200 x 400 mm^2, each point neighboring another by 100 mm. The term was given in P_{CR} where C = (1,2,3) and R = (1,2,3,4,5). 'C' and 'R' stands for column and row, respectively

For each center of the image data set from the target, p_{img}^{tgt}, is calculated as the center of target. The transformation matrix for relating the image to the robot end effector's Cartesian coordinates, T_{ref}^{img}, is determined by the pair-point matching method, which is implemented using Equation 2.6 and 2.7. Therefore, the localization error is

$$Localization\ Error = \left| P_{ref}^{tgt} - T_{ref}^{img} \cdot P_{img}^{tgt} \right| \tag{2.9}$$

Area-per-spot test

The area-per-spot test is performed to verify the effective and consistent detection capability of the proposed system. Under the assumption that a uniform distribution of laser irradiation is achieved within the target, this result value is used to measure the quantitative omission or overlap rate. The spots are the locations within the target area where the laser irradiation treatment is to be implemented, whereas the area is the target's size within the image frame. Once the target is set, the system can automatically count and identify the exact locations for laser irradiation. Different sizes of squares, right triangles, and circles were selected and tested for five rounds, with a total of 90 samples collected. For each figure, a round set consisted of detecting the smallest to largest size in a consecutive manner, and with no one figure being tested

more than once per trial. Five set of rounds were tested. Arbitrarily shaped figures were also tested by measuring their approximate areas. The figures were manually drawn on graph paper with non-reflective red marker. The area approximation is measured in terms of a 5 x 5 mm^2 grid. The area that completely fills 25 mm^2 in read is considered 25 mm^2, whereas any uncompleted area in red was considered half of the completed area, which is 12.5 mm^2. The total area constitutes the sum of those areas. Four samples were used in the trial.

2.2. Clinical trial

This study is composed of development of the treatment system and its clinical trial to verify its efficacy. This section is dedicated to explaining the method, process, and contents of the clinical trial. Until now, there has not been a clinical trial under the assumption of uniform distribution of laser delivery. Partly this isn't any available tool or device that can perform it on wide area. Also, there are continued effort to improve the efficacy of treatment and the effect of mechanical properties such as wavelength, pulse duration, spot size, fluence and method of skin cooling after the irradiation are being assessed in various clinical studies[3, 27-33]. However, physicians' delivery skills are rarely described and discussed. The low-power laser treatment such as laser hair removal has its foundation based on the theory of selective photothermolysis. As mentioned in introduction of this paper, the overlap percentage and omission affects the efficacy of laser treatment and clinical result of laser delivery that does not assume the uniform distribution has low reliability. The clinical trial was conducted to answer the question whether the reliable uniform distribution of laser delivery will show better treatment efficacy than physician directed laser delivery. Since laser hair removal is a one of the most widely used laser treatment, it was chosen as the laser device.

The study was conducted in accordance with the 2013 revision of

the Declaration of Helsinki with medical device clinical trial approval from Korea Ministry of Food and Drug Safety, Approval No. 474 and clinical trial approval from Seoul National University Hospital, IRB No.: D-1303-017-470

2.2.1 Preparation and methods

Subjects

Six healthy male subjects 20-40 years of age with Fitzpatrick skin types III-IV and black hair were registered in the study. All subjects were given careful explanations about the experiment, and voluntarily registered to participate in the study. Each subject was required to satisfy all of the inclusion and exclusion criteria. The inclusion criteria were a minimum of 35 hairs within an area of 90 x 120 mm^2 on each thigh, and an equivalent amount of hairs on both thighs. The exclusion criteria were any history of LHR, electrolysis, or other hair removal practice on the test site; any intake of hair growth or wound-healing medicine; any intake of oral retinoid within the previous 12 months; any previous formation of keloid scars; and the use of medicine that could affect skin regeneration.

Table 2.3 shows the treatment schedule for each visit. The fundamental treatment conditions used in both the automatic and physician-directed procedures were the same. The treatment areas

were 90 x 120 mm^2 areas on both thighs. Figure 2.29 shows the LHR system and the subject position during robot treatment. Figure 2.30 shows the subject during the manual treatment. Figure 2.31 contains a flow chart indicating the order of subjects' activities. The flow chart displays every steps of subject had to take prior to the clinical trial.

Figure 2.29 Laser treatment system and patient are ready for clinical trial. The subject sits comfortably on a cushion and lean back against the wall while the treatment is conducted.

.

Figure 2.30 The subject sitting on the bed during the physician-directed treatment.

Table 2.3 Subjects' treatment schedule.

Activities	Screen visit	1st visit (1st Day)	2nd visit (D+2 weeks)	3rd visit (D+5 weeks)	4th visit (D+7 weeks)	5th visit (D+11 weeks)
Inclusion and exclusion criteria	○					
Informed consent	○					
Photo session		○	○	○	○	○
Shave		○	○	○	○	
LHR by the system		○	○	○	○	
LHR by the physician		○	○	○	○	
Physician’s diagnostics		○	○	○	○	○

* 1st day is denoted as D

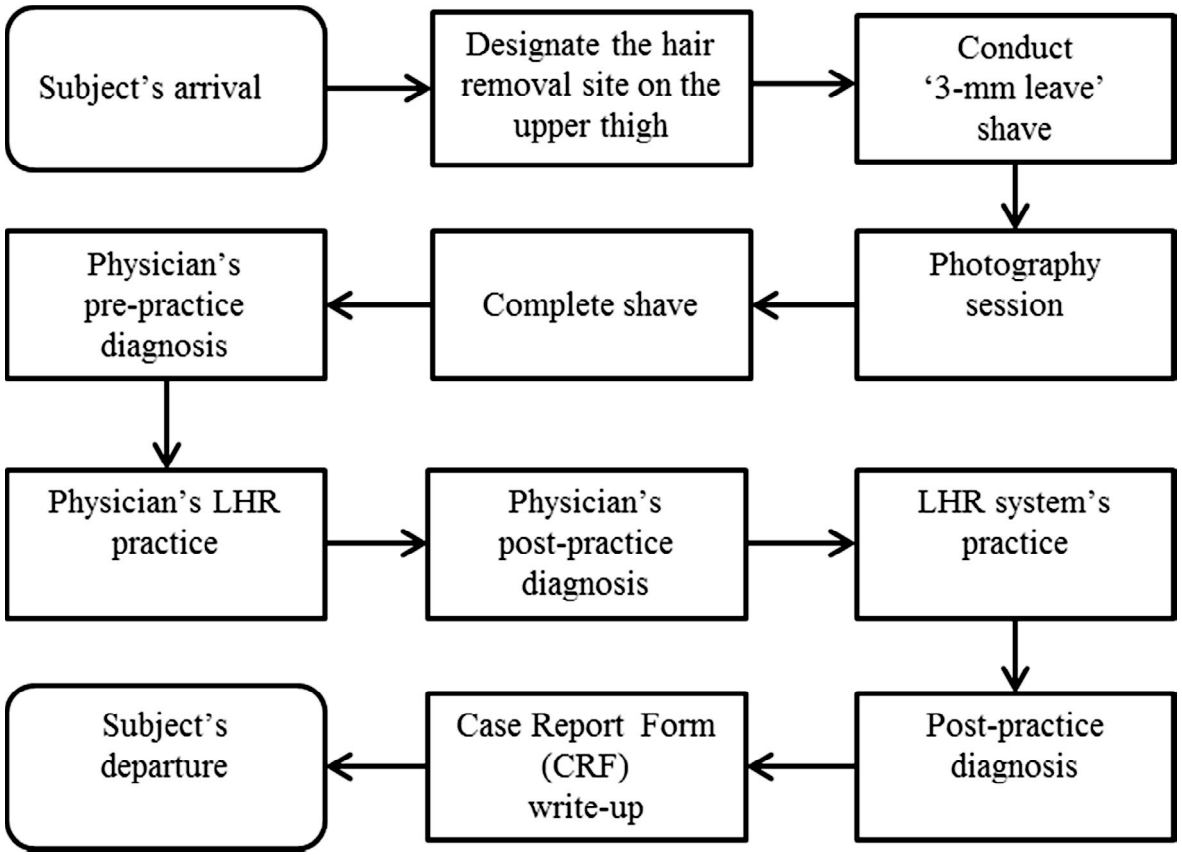

Figure 2.31 Flow chart indicating the order of subjects' activities.

For each subject, one thigh was treated by a physician specializing in dermatology, and the equivalent site on the other thigh was treated using the automatic LHR system. The decision of which thigh (left or right) would receive each treatment type was decided according to random numbers generated using the SPSS 21.0 software program (IBM-SPSS Inc., Chicago, IL). The four edges of the treatment site were marked with a nontoxic color marker and were re-marked during the following visit for visual confirmation. The location of each edge was traced according to both a photograph taken during the first visit and biological skin characteristics such as scars and moles. A "3 mm leave" hair shave was conducted using an electrical shaver (ES-148; Panasonic, Osaka, Japan) with a 3 mm guard on. This process was intended to ensure accurate hair counts on photographs. The number of hairs counted from the first visit photo was set as the initial amount of hair, or baseline. Subsequently, the hairs were completely shaved using the same electrical shaver.

The treatment processes were not conducted simultaneously. Rather, the physician-directed treatment was performed first, followed by the LHR system. The interim period between the procedures was < 30 min., and throughout the treatment, the physician was uninformed and unaware of the treatment duration

and number of irradiation shots of the LHR system throughout the treatment sessions. The physician used a "pick and place" technique to minimize laser irradiation omission and overlap. The automatic LHR system, also used "pick and place" technique, in which each irradiation spot was centered 6 mm horizontally and vertically from the centers of neighboring spots; this distance was recommended by the LHR device manufacturer's manual. Both treatment methods followed a "one path rule" to provide irradiation in a continuous manner without returning to the previously irradiated area. Both methods also incorporated the Tria Plus (Tria Beauty, Dublin, CA), a home-use level 5 LHR device with the following specifications: laser irradiation fluence, 20 J/cm^2; wavelength, 810 nm; and pulse duration, 350 msec.

The 1st through 4th visits occurred at intervals of roughly 2 weeks (the third visit was held on week D+5 because week D+4 included Korean national holidays) and included photograph sessions, shaving, and LHR treatment. The fifth visit included only a photograph session.

2.2.2. Performance indicators

Outcomes were represented in terms of the number of irradiation shots, treatment duration, and hair removal rate. The measures focused on the quantitative hair counts at each visit. The primary effectiveness assessment as the hair removal rate, calculated as the difference between the initial baseline and the number of hairs counted on the 5^{th} visit of each subject as follows:

$$Hair\ Removal\ Rate = \frac{(baseline\ - 5^{th}\ visit)}{baseline} \times 100 \qquad (2.10)$$

Hairs were counted on photographs taken with a Nikon DSLR D5100 camera (Nikon, Tokyo, Japan) with an AF-S Micro NIKKOR 40 mm 1:2.8G lens. The camera was fixed on a tripod, and photographs were taken at a fixed distance in aperture-priority auto mode (A-mode) and were stored at a resolution of 4928 x 3264 pixels/mm^2. Adobe Photoshop CC 2014 (Adobe Inc., San Jose, CA) was used to open the photograph files. Each hair was counted with naked eyes and clicked as a point. The zoom-in function was used when required.

3. Result

3.1. Result of laser delivery skills among physicians

We used a laser beam detection kit to visualize the locations of the laser beams during laser treatments by eight physicians.

The investigation of the diversity of laser delivery skills among physicians provided quantitative data showing how differently physicians performed when given the same task and work environment. The clinical trial environment is introduced in Section 1.3.

The assessment parameter d_n denotes the distance between adjacent laser spot centers. The characteristics of d_n are distinct from the other factors, and allow the performance of each method to be assessed. d_n is the most basic indicator of laser delivery traits and shows how densely the laser irradiation was made on the LDM.

Table 3.1 shows the average omission, overlap percentages, $d_{n,}$ number of shots, and treatment duration of each physician. Each physician performed ten laser delivery trials. The physicians who had low $d_{n,}$ had a high number of shots, high overlap percentage, and high treatment duration. Physician 4 is a good example of this case.

Table 3.1 Omission percentage, overlap percentage, d_n, number of shots, and treatment duration from each physician.

Physicians	Omission percentage (δ_0)	Overlap percentage (δ_z)	d_n	Number of shots	Treatment duration (sec.)
	Average ± S.D.	Average ± S.D.	Average ± S.D.	Average ± S.D.	Average ± S.D.
1 (Clinic A)	17.8 ± 4.2	11.1 ± 2.8	10.1 ± 1.6	142.3 ± 10.7	166 ± 11.8
2 (Clinic A)	14.6 ± 2.2	13.2 ± 2.5	9.8 ± 1.4	151.2 ± 5.0	263 ± 59.0
3 (Clinic A)	11.6 ± 5.2	29.3 ± 7.5	8.4 ± 1.7	187.3 ± 18.7	217 ± 23.5
4 (Clinic A)	9.5 ± 1.6	51.0 ± 17.9	6.8 ± 1.7	251.8 ± 60.0	333 ± 81.3
5 (Clinic B)	18.9 ± 2.1	17.2 ± 1.8	8.9 ± 1.9	150.9 ± 1.9	207 ± 22.0
6 (Clinic B)	20.4 ± 4.1	14.0 ± 5.1	9.7 ± 1.9	151.1 ± 15.5	171 ± 20.4
7 (Clinic B)	17.6 ± 5.4	18.4 ± 9.3	8.4 ± 2.0	156.9 ± 22.4	178 ± 28.3
8 (Clinic B)	22.1 ± 3.8	9.0 ± 3.3	10.1 ± 1.8	135.1 ± 9.0	166 ± 12.7
Total	16.6 ± 5.5	20.4 ± 15.1	9.0 ± 1.8	165.8 ± 42.9	213 ± 67.4

* S.D. stands for standard deviation

Table 3.2 Summary of the statistical test results for the omission percentages, overlap percentages, and number of shots among the physicians.

Number of cases	Omission percentage (δ_0) (Dunnett T3, p−value<0.05)	Overlap percentage (δ_z) (Mann−Whitney, p−value<0.0018)	Number of shots (Mann−Whitney, p−value<0.0018)
Statistically different	12	14	13
Statistically not different	16	14	15
Total number of cases	28	28	28

All physicians were compared, creating 28 different combinations. ANalysis Of VAriance (ANOVA) and posthoc using Dunnett T3 analysis showed that omission percentages were statistically different (p−value was set to be 0.05) in 12 of 28 cases. Based on the Mann−Whitney test with posthoc Bonferroni adjustment analysis of each case the overlap percentages in 14 of 28 cases were statistically different (p−value: 0.0018). Table 3.2 summarizes these results. The number of shots performed by each physician and trial was analyzed, and the results showed that 13 of 28 cases were statistically different even though physicians irradiated the same target size (p−value: 0.0018).

Table 3.3 Average and standard deviation of the omission percentage, overlap percentage, and number of shots of each clinic.

Clinic	Omission percentage (δ_0) Average ± S.D.	Overlap percentage (δ_z) Average ± S.D.	Number of shots Average ± S.D.
A	13.4 ± 4.7	26.1 ± 18.7	183.2 ± 53.3
B	19.7 ± 4.2	14.6 ± 6.5	148.5 ± 16.1
Statistical difference	Yes (Independent t-test, p-value <0.05)	Yes (Mann-Whitney test, p-value <0.05)	Yes (Mann-Whitney test, p-value <0.05)
t-value	6.3	3.6	3.9

* S.D. stands for standard deviation

The data from the physicians of Clinic A and Clinic B were statistically different in terms of the omission percentage, overlap percentage, and number of shots (Table 3.3), indicating variation in performance. The omission percentage was analyzed using the parametric method, whereas the overlap percentage and the number of shots were analyzed using the non-parametric method. The results of the analyses suggested that the two clinics had a difference in performance in terms of these three criteria.

3.2. Performance of the developed system

3.2.1. Image processing and work planning

The target detection result of various arbitrary shapes is shown in Figure 3.1, and the GUI panel, which presents the sequence of operation, is shown in Figure 3.2. Filled out black regions are completed irradiated zones, whereas yellow hollow circles are the to-be-irradiated zones. The "pick and place" movement used to implement the laser treatment starts from top left to right, and then moves to the next row. The "operation steps" group, located at the bottom left, provides all the data that are required for controlling the robot. On screen, "Tria displacement" is the distance between one center of a circle and another. "Total No. of Pick and Place" is computed and displayed as soon as the "Practice" button is activated. The completion progress bar and percentage are displayed in real time. Once the last spot is completed, the robot's end effector moves to the initial position.

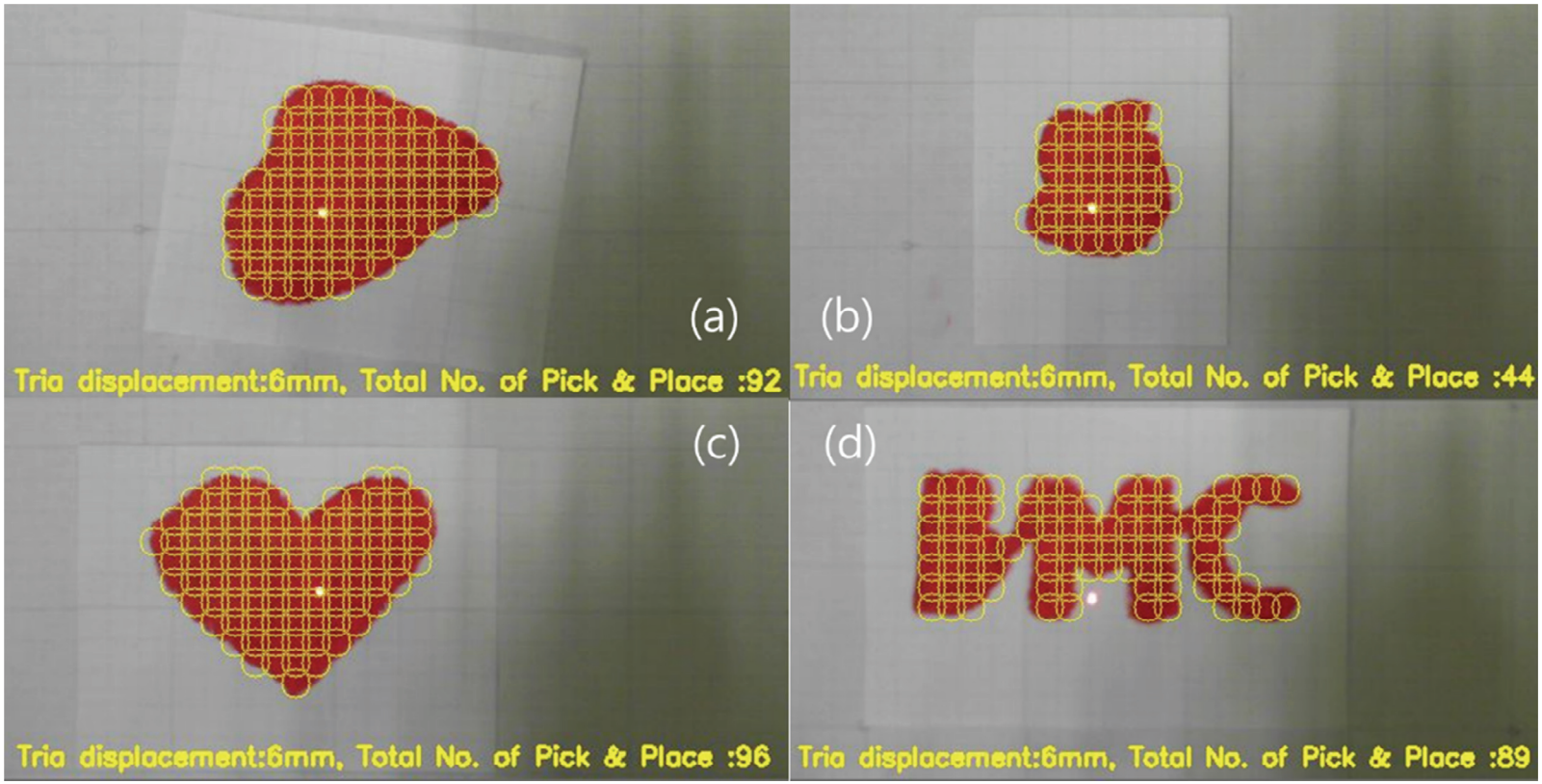

Figure 3.1 Various types of arbitrary shaped target detection result with grids. From (a) to (d), the 'area per spot' was measured 38.04, 38.63, 38.02, and 38.20 mm^2/spot, respectively.

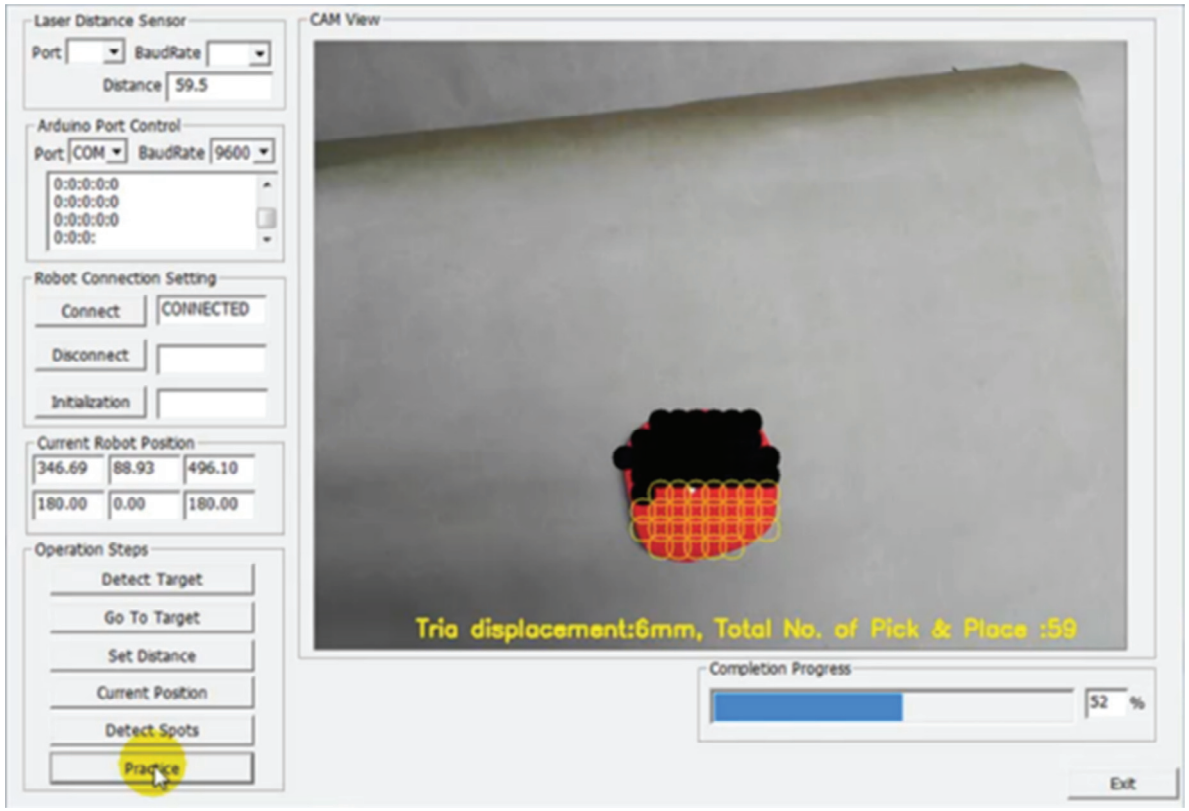

Figure 3.2 Graphic user interface (GUI) panel. Filled out black regions show irradiated treatment and yellow hollow circles are to-be-irradiated spots.

3.2.2. Localization−error test

One hundred and fifty samples were collected successfully, and the laser beam from the distance sensor was identified near each target's center point. The distance between the laser distance sensor and the target was maintained at 250 mm. Table 3.4 is the localization error result which depicts the test result of 10 rounds of 15 different points. The lowest error was taken from P_{32} (mean error: 0.40 mm) and the highest error was from P_{22} (mean error: 1.79). The time required for the entire procedure per trial was typically < 40 sec, whereas it took < 1 sec to detect the target from the initial position, and the coordinate value of the center point of the target was identified in real time on the GUI panel. The rest of the time spent was attributed to the robot's movement and the clicking operation buttons on the GUI panel.

Table 3.4 Localization-error test result.

	Mean (mm)	S.D.
P_{11}	1.76	0.00
P_{12}	1.74	0.30
P_{13}	1.34	0.00
P_{14}	0.45	0.00
P_{15}	0.75	0.00
P_{21}	1.33	0.00
P_{22}	1.79	0.00
P_{23}	0.44	0.00
P_{24}	0.66	0.00
P_{25}	1.25	0.00
P_{31}	1.02	0.00
P_{32}	0.40	0.00
P_{33}	1.29	0.00
P_{34}	0.48	0.00
P_{35}	0.99	0.00

* S.D. stands for standard deviation

3.2.3. Area-per-spot test

The results for the arbitrarily shaped figures from Figure 3.1 are also presented on Table 3.5.Various shapes and sizes of ideal form figures, including squares, right triangles and circles, had averages of 37.89 cm^2/spots (SD: 2.67, n = 40), 38.03 cm^2/spots (SD: 2.10, n=30) and 38.21 cm^2/spots (SD: 0.65, n = 20), respectively (Table 3.6). The speed of the robot movement is manually adjustable. By fixing its acceleration and deceleration at 4.41 m/sec^2, it took <3 sec to move from one spot to another.

Table 3.5 Area-per-spot test for arbitrary shapes of Figure 3.1.

Arbitrary shaped figures	Area measured in approximation (mm^2)	Area / Spots (mm^2 /spots)
Fig. 24 (a)	3500	38.04
Fig. 24 (b)	1687.5	38.35
Fig. 24 (c)	3650	38.02
Fig. 24 (d)	3425	38.48
Average	N.A.	38.22
S.D.	N.A.	0.19

* S.D. stands for standard deviation

Table 3.6 Area-per-spot test for squares, right triangles, and circles.

Square (mm^2)	Area / Spot (mm^2 / spot)	R. Triangle (mm^2)	Area / Spot (mm^2 / spot)	Circle (radius) (mm)	Area / Spot (mm^2 / spot)
30 x 30	36.00	50 x 50	34.72	20	38.07
40 x 40	44.44	60 x 60	40.00	30	37.20
50 x 50	39.06	70 x 70	37.12	40	38.66
60 x 60	36.00	80 x 80	41.02	50	38.81
70 x 70	37.12	90 x 90	38.57		
80 x 80	37.86	100 x 100	36.76		
90 x 90	36.00				
100 x 100	36.63				
Average	37.89	Average	38.03	Average	38.21
S.D.	2.67	S.D.	2.10	S.D.	0.65

* S.D. stands for standard deviation

3.3. Clinical trial result

Treatment duration and laser irradiation shots

All six subjects successfully and safely completed the clinical trial without any long-term side effects. A total of 96 data samples were collected successfully during the 1st through the 4th visits, and each datum was measured accurately as numbers of seconds and irradiation shots. Table 3.7 shows the average treatment durations and actual numbers of irradiation shots administered by the automatic LHR system and the physician. Speed of robot is adjustable and purposely slowed down.

Table 3.7 The average treatment duration of the 1st through 4th visits and the numbers of irradiation shots administered by the system and physician.

	Average from 1st to 4th visit			
	LHR System		Physician	
	Duration (mm:ss)	Shots irradiated	Duration	Shots irradiated
Subj.1	18:58	266.2	3:00	66
Subj.2	18:58	248.5	3:00	70.2
Subj.3	17:24	254.2	2:54	67.7
Subj.4	19:01	269.5	3:27	81.2
Subj.5	18:50	257	3:09	65.5
Subj.6	17:53	262.5	3:37	87
Avg.	18:30	260	3:11	73
SEM	0:33	5.7	0:15	5.9

* The robot's speed is adjustable and was purposely slowed for subjects.

**Standard error of the mean (SEM)

The average treatment duration and number of irradiation shots administered by the automatic LHR system were 18 min, 30 sec [standard error of the mean (SEM): 33 sec] and 260 shots (SEM: 33 shots), respectively. The subjects' thighs had different irradiation spots differed; however, nearly 288 spots were detected. The average treatment duration and number of irradiation shots administered by the physician were 3 min, 11 sec (SEM: 15 sec) and 73 shots (SEM: 5.9 shots), respectively. Figure 3.3 shows the ideal geometric placement of irradiation spots, the programmed placement of irradiation spots by the automatic LHR system, and the estimated irradiated spot placement by the physician. Notice that Fig 3.3 (c) includes an area outside of the circles that is considered an un-irradiated area. This figure contains 70 circles that represent the average placement of the physician's irradiation shots within the 120 x 90 mm^2 area after excluding the two highest outliers from the data.

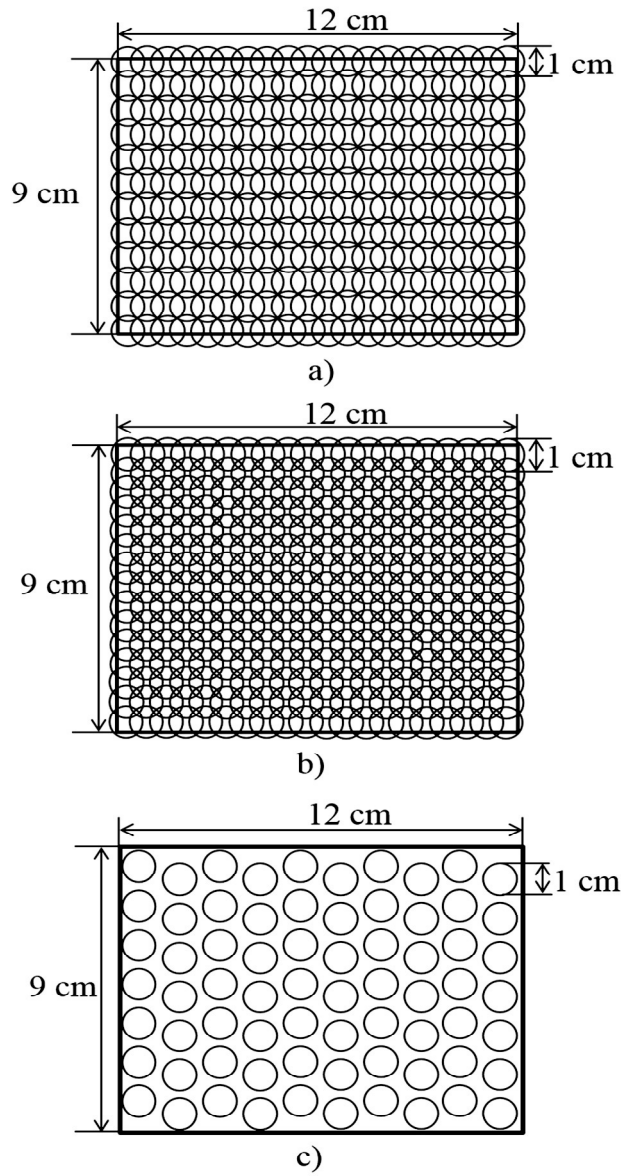

Figure 3.3 Laser shots. (a) ideal geometric placement, (b) programmed irradiation spots coverage, (c) estimated placement of physician-directed irradiation coverage.

Hair counts and removal rates

Figure 3.4 depicts the clinical results of the two methods at the 1st (baseline) and 5th visits. It is the pre- and post-hair removal results for Subject 5. The area within the red bracket is 90 x 120 mm^2. (a and b) demonstrate the results after the 1st and 5th visits with physician-directed treatment. (c and d) demonstrate the results after the 1st and 5th visits using the LHR system. Table 3.8 presents the numbers of hairs counted on the photographs from the baseline to the 5th visit. Figure 3.5 depicts how hair removal differed from the baseline to the 5th visit. The average hair removal rates were 49.0% (SEM: 9.9 %) and 29.5% (SEM: 9.8%) with the automatic LHR system and physician-directed treatment, respectively. Figure 3.6 depicts the uniformly distributed laser irradiation by the robot-assisted system. The size of the laser delivery area is 120 x 90 mm^2. It is the reconstructed image of Figure 3.3 (b) in 3D using Gaussian normal distribution as intensity of energy distribution. Figure 3.7 depicts the laser irradiation by physician. The size of the laser delivery area is 150 x 100 mm^2 and it is the reconstructed 3D image of Figure 1.7 (d). One must notice that only the treatment duration and number of shot can be measured as a record in clinical trial when patient. There is no method to trace exact location and its irradiation time. Therefore, the results of laser beam irradiation location received from laser beam detection kit were reconstructed in 3D image to see the

uniformity of both methods.

Safety

Subjects were evaluated by the clinician prior to each treatment, and no adverse effects were reported from either procedure other than transient erythema at the treatment site, which usually disappeared within a few hours after treatment. The safety sensor located around the laser output window operated adequately; an encounter with any force exceeding 0.49 N (50 g) activated the sensor and directed the robot to return automatically to the initial position.

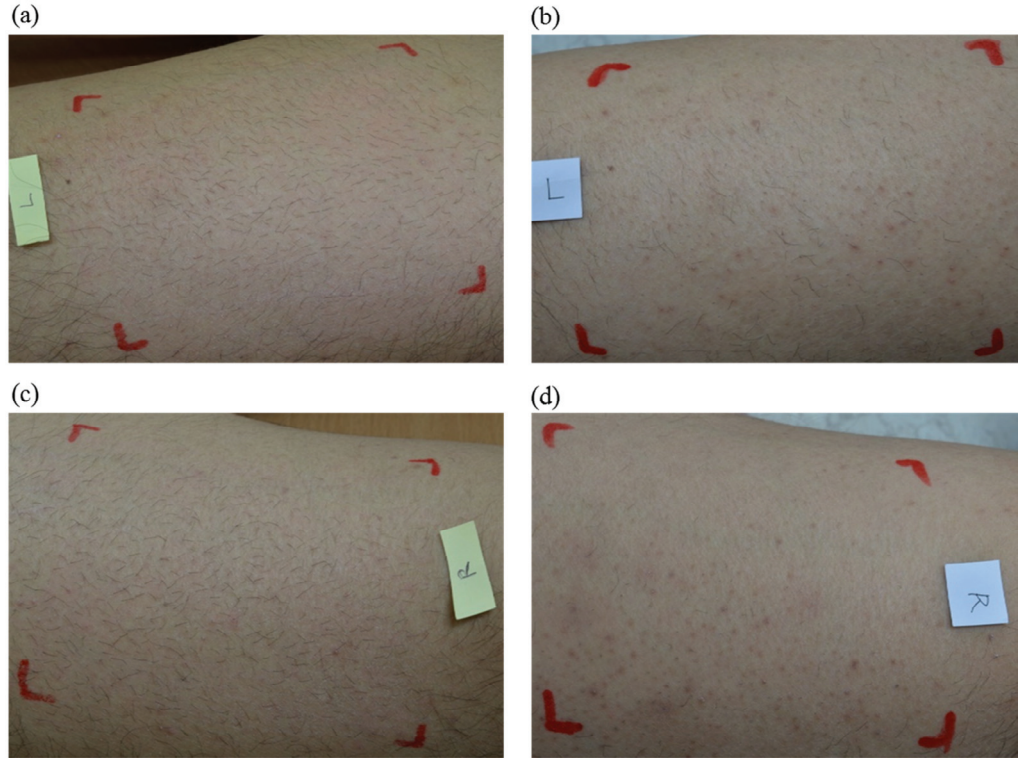

Figure 3.4 Pre- and post- laser treatment results of subject 5. The area within the red bracket is 90 x 120 mm^2. (a and b) demonstrate the results after the 1^{st} and 5^{th} visits with physician directed treatment. (c and d) demonstrate the results after the 1^{st} and 5^{th} visits using the robot-assisted treatment system.

Table 3.8 Hair counts and removal rate of two different methods.

	1st Visit (Baseline) 1st Day		2nd Visit D + 2 weeks		3rd Visit D + 5 weeks		4th Visit D+ 7 weeks		5th Visit D + 11 weeks		Removal Rates	
	LHR System	Physician	LHR System	Physician	LHR System	Physician	LHR System	Physician	LHR System	Physician	LHR System	Physician
Subj.1	588	584	458	368	350	430	284	303	247	316	58.0	45.9
Subj.2	818	910	631	812	752	856	565	910	527	747	35.6	17.9
Subj.3	510	603	366	495	370	558	354	405	328	498	35.7	17.4
Subj.4	420	501	423	439	319	422	353	472	199	329	52.6	34.3
Subj.5	873	853	615	717	497	707	464	586	345	583	60.5	31.7
Subj.6	614	598	507	568	332	499	301	425	298	421	51.5	29.6
									Avg. Removal Rate		49.0	29.5
									Standard Error of the Mean (SEM)		9.9	9.8

*1st Day is denoted as D

** The 3rd Visit was held on D+5 week since the 4th week was Korean national holidays.

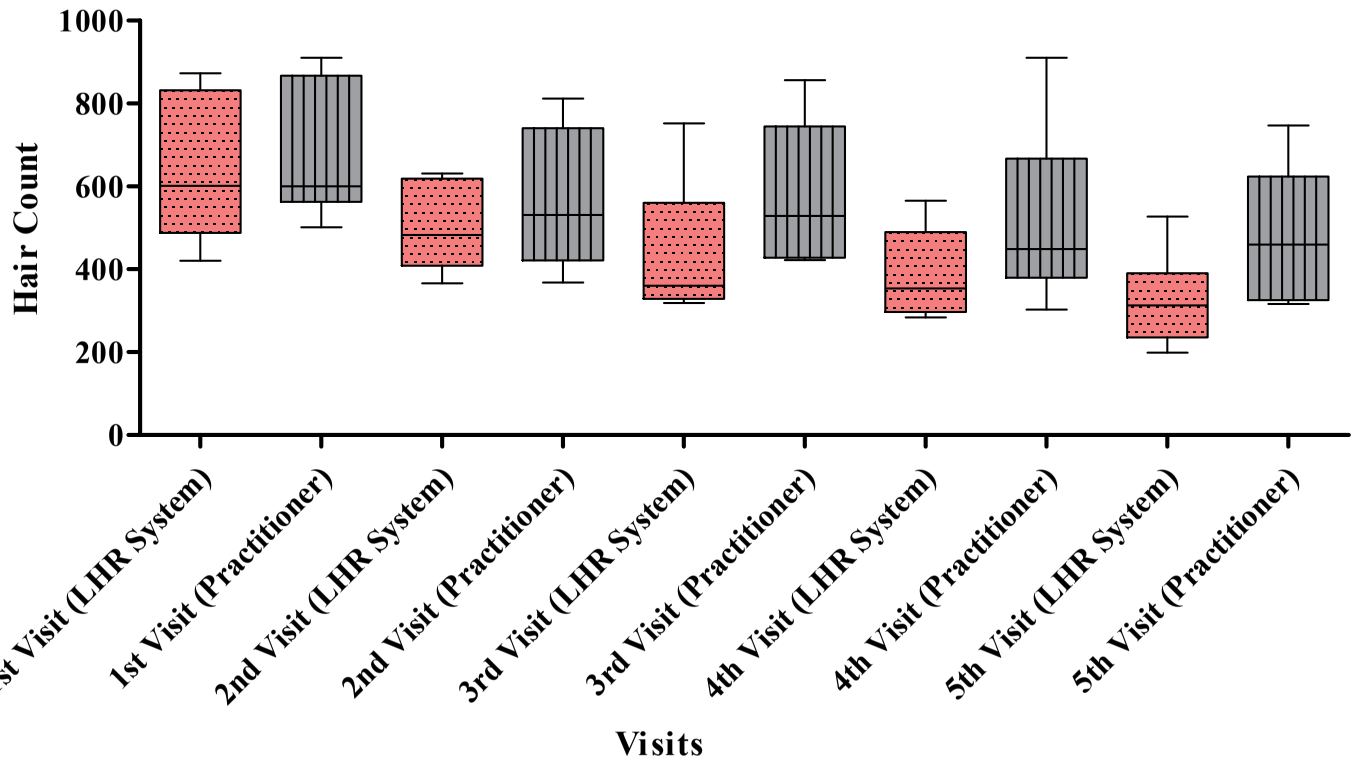

Figure 3.5 Hair removal result between the system and treated by physician. Box plots indicate the median number of hairs remaining and interquartile ranges; whiskers indicate the minimum and maximum values.

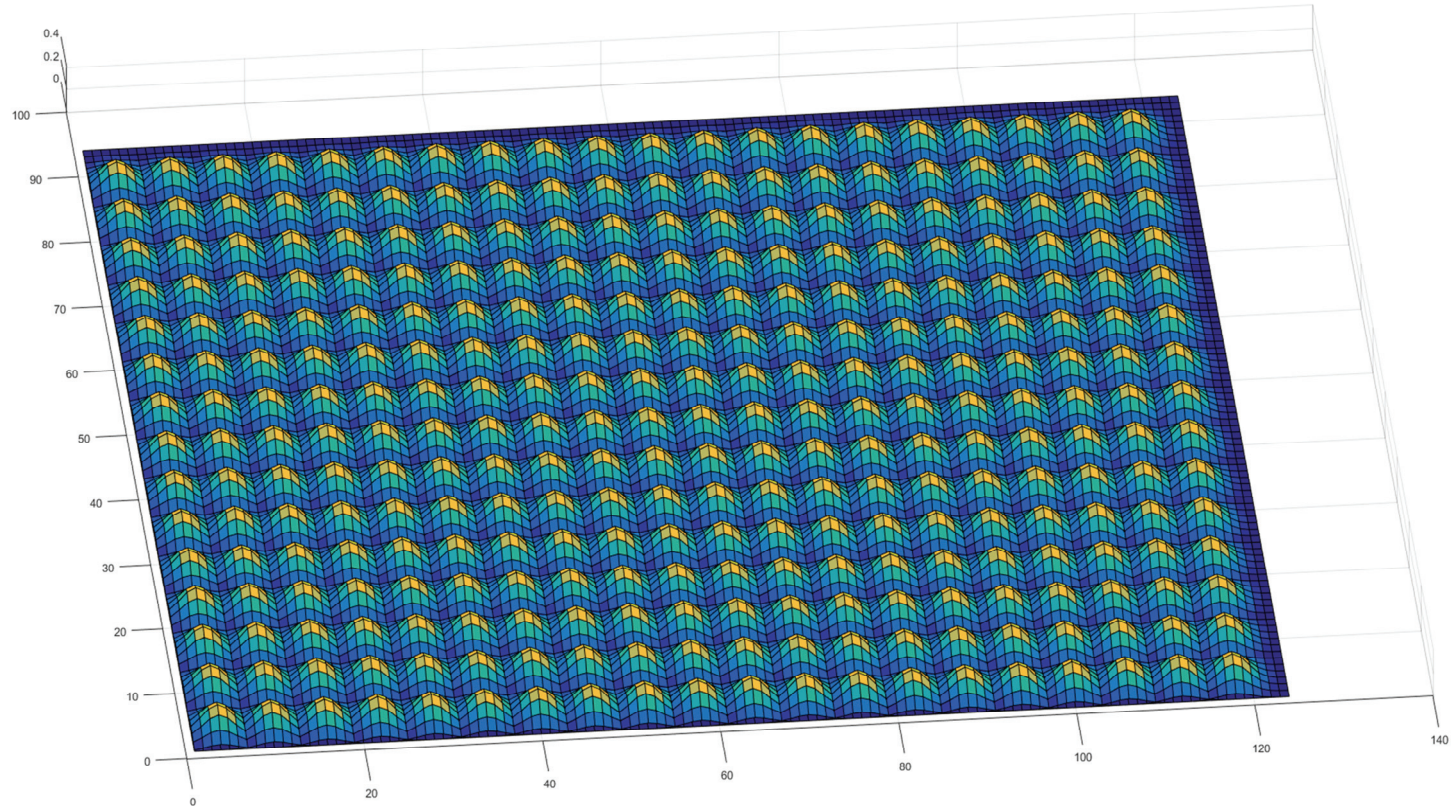

Figure 3.6 Uniform distribution of laser irradiation by robot-assisted system. Size of 120 x 90 mm^2. Reconstructed Figure 3.3(b) in 3D using Gaussian normal distribution as energy distribution of laser. The displacement distance between the spots is 6 mm.

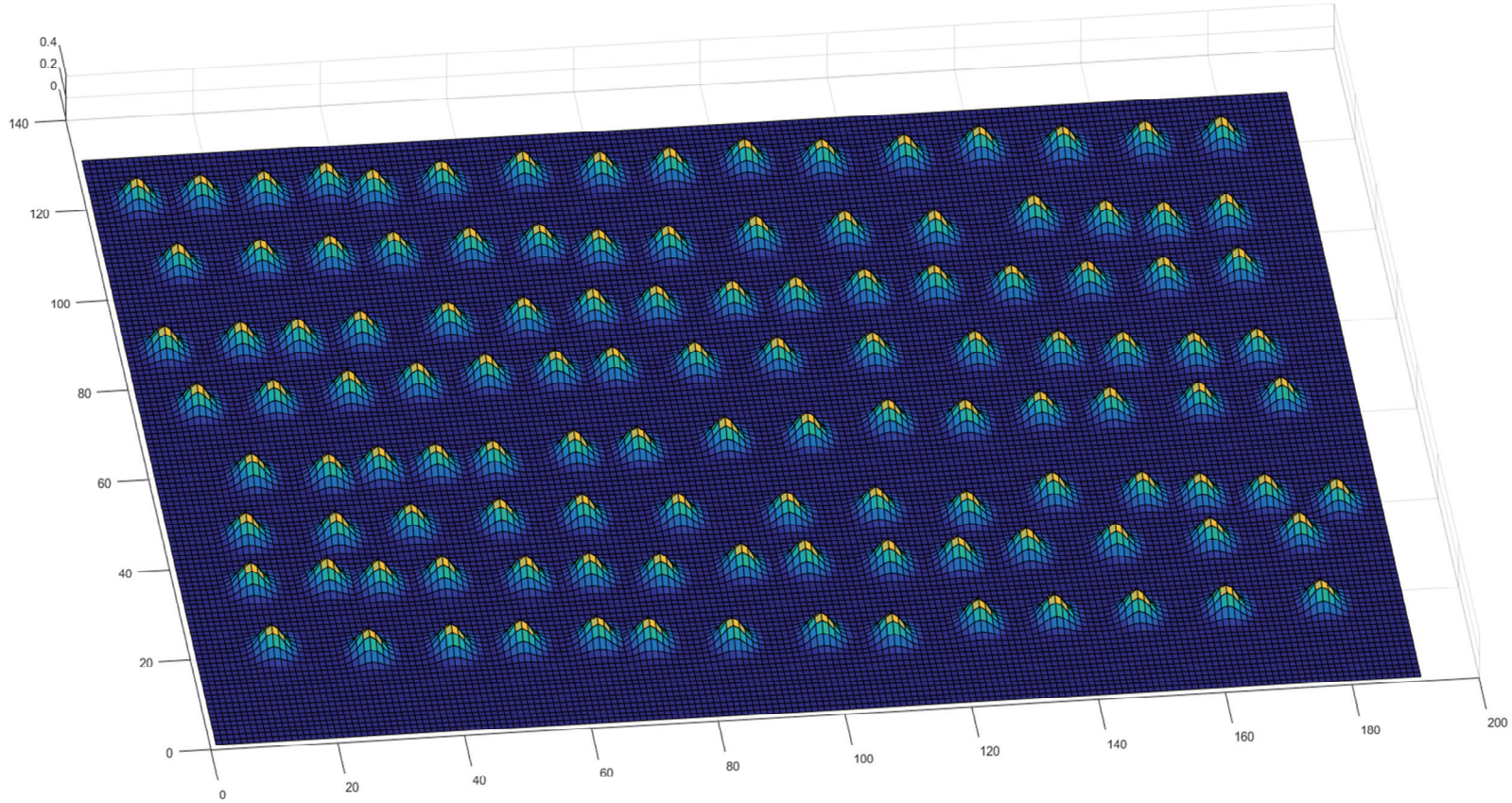

Figure 3.7 Laser irradiation by physician. Size of 150 x 100 mm^2. Result of Figure 1.7(d) reconstructed in 3D.

4. Discussion

It is extremely difficult to discern the location of irradiation with eye during laser treatment. A group of researchers proposed a thermo-vision camera to visualize the heat change in tissue to trace the laser irradiation indirectly to resolve this issue.[34-36] However, the thermo-vision camera is a less practical approach because of most laser treatment devices, including the laser hair removal devices at professional clinics have cooling tips built around the laser irradiation tip, which lessens the efficacy of the thermo-vision camera. The results of the evaluation of physicians' laser delivery skills suggest that a uniformly distributed laser irradiation is very difficult to achieve, and the displacement distance that determines the omission and overlap percentage depends completely upon the perception and skills of the physician. Table 3.1 shows that the physicians who had low d_n had a high overlap percentage and longer treatment duration, whereas those who had high d_n had a high omission percentage and shorter treatment duration. All physicians had a different value of d_n and its standard deviation. However, the proposed robotic system can perform an ideal uniform laser delivery with a programmed d_n and a standard deviation that approaches zero, regardless of variations in the external environment.

The robotic system has many obstacles and limitations to be overcome, such as the treatment duration, the ability to treat on rapidly changing 3D curvatures, and the ability to irradiate the patient regardless of their movement. The treatment duration for the system was, on average, six times greater than for the physician-directed treatment. However, one cannot directly judge the success from differences in the treatment duration because the performance of the physician was often a result of poor technique. The physicians should have applied >260 more shots to achieve an ideal treatment; instead, the physicians' results had a high omission percentage. There was no limit on the duration of treatment for the physician and had the physician taken longer and performed more shots omission would have decreased, but the overlap percentage would have increased. The laser delivery skills of the physicians were not the gold standard; the robotic system could achieve a uniformly distributed laser irradiation while the physicians could not. This research assumed that the treatment was conducted in 2D space and the patient was immobile. The patients sat on the table without movement during the clinical trial, but this limitation should be remedied in future development. An integrated system that is specified for the sole purpose of laser treatment should be developed as the next research goal. The end-piece should also be integrated with the end-effector of the robot as one body. Development of a training system that will enhance physicians'

delivery skills is also important since it can benefit patients without increasing medical cost to the clinics and doctors.

Among the factors that contributed to the experimental error margin, it is suspected that the laser beam size (circle, d = 2 mm) from the laser distance sensor is the most significant. The laser beam provided visual guidance for calibrating the pair-point matching method. Serious efforts were made during the calibration to take precise measurements, but it would be much more effective to adopt a laser beam pointer with a smaller diameter, which would provide a finer measurement by reducing the localization error. The low standard deviation values of each point are the result of camera coordinate values that are extracted in terms of whole numbers, whereas the robot's coordinate values are given to hundredths of a decimal place. The relatively high standard deviation on P_{12} might be the result of the test environment; for example, a ceiling light directly above the point where the light was reflected most could result in oscillation in the detection of the target's center point.

The area-per-spot test results for detection capability were consistent in both ideally formed and arbitrarily shaped figures. Given a radius of 5.5 mm, the LOW area for Tria Plus is 95.03 mm^2. The experimental result presented in the various figures measured using the proposed system is ~38 mm^2/spots, which is ~2.5 times as much as the difference. Adopting this system to other LHR

devices with a square shaped LOW would increase the ratio.

The current system leaves some undetected areas along the edges because they lack sufficient color regions to be considered an irradiation site. The image processing algorithm creates the lattices on the detected target, which has >60% of its contents. Because the proposed system is primarily aimed at treating a wide coverage area, where sensitive regions are not included, the user may employ manual treatment along the edge line.

The results of the clinical study confirm the effectiveness and safety of our robot-assisted LHR system through comparison with the results obtained with physician-directed LHR. The automatic LHR system achieved near-uniform laser irradiation distribution. The curvature of the human thigh caused the system to have a lower detection rate relative to that achieved on a flat surface (i.e., 300 spots). However, the system detected ~288 spots for the given treatment area on the thigh.

In some subjects, the laser device on the LHR system misfired even when the device tip was placed directly in contact with the skin for a sufficient duration of time for irradiation. Subject 2 experienced relatively more misfires during the first and second visits, compared with other subjects, and this was attributed to the subject's perspiration, which led to malfunctioning of the device's irradiation sensor. When a series of misfires was detected, the

system was paused, the laser device window and sensor area were cleaned with wet tissue and dry tissues, and the subject's area of perspiration was cleaned with wet tissue and dry tissue before resuming treatment. These measures successfully and significantly reduced the number of misfires, and the number of irradiation shots returned to within the normal range during the third and fourth visits. Such misfire issues should be remedied before incorporating the professional laser treatment device soon.

As demonstrated in the results, there was a considerable difference in the average treatment durations of the two methods. The subjects were uncomfortable with the high robot movement speed, and, therefore, the speed was adjusted to a comfortable and satisfactory level. This change consequently elongated the automatic LHR treatment duration to nearly six times longer than that of the physician-directed treatment. Further optimization of the treatment speed and subjects' perceived comfort level will be addressed following the introduction of commercial research and development.

It is important to notice that the physician was unable to perform uniform distribution of laser delivery even though he was given the freedom to start and end his laser delivery. The physician-delivered much less than the idealistic number of irradiation compared to the robot-assisted laser treatment system. If the

physician displayed better performance by delivering more amounts of irradiation and near to idealistic laser delivery, more time must have taken for him/her. According to the research on the evaluation of laser delivery skills, physicians who spent more time on laser delivery showed low omission percentage, however, they also showed a high percentage of overlap percentage. It is plausible to imagine that physicians who display high omission percentage have low overlap percentage and vice versa. If the physician focuses on lowering omission rate during laser delivery, it may raise the overlap percentage. Since both the cases of high omission percentage and high overlap percentage can be problematic, idealistic laser delivery is very difficult for human to perform.

The LHR system provides consistent irradiation not only in terms of uniform distance but also the number of irradiation shots. Table 8 shows that although the LHR system and physician-directed treatment had equivalent standard error of the mean (SEM) values (5.7 and 5.9 for the LHR system and physician, respectively), the average number of irradiation shots delivered by the LHR system was nearly 3.5 times greater than that delivered by the physician. The SEM of the LHR system would have been even lower if the misfires were reduced or absent.

These differences in hair removal results with the same device may be because of the influence of human factors (e.g., proficiency,

fatigue, the laborious and time-consuming nature of the procedure, and inability to detect the exact locations of irradiation). Therefore, reliable LHR results are expected with the proposed automatic system. As multiple skin-related treatments (e.g., LHR, pigmentation, tattoo removal, scar resurfacing, acne treatment) are conducted using photo-medicine, the proposed system is expected to be widely applicable.

5. Conclusion

In this research, two methods of achieving uniform distribution of laser irradiation were introduced, and both methods showed promising results to be used by physicians.

LBDK, a laser irradiation analysis toolkit, provides the omission and overlap rate of the physicians' laser delivery skills. Through this measurement system, the diversity of laser delivery skills among physicians was confirmed and verified through statistics. It's development was inexpensive but it proved to be highly effective. The system is expected to be useful as it can show the progress in a user's improvement when continuously used.

A robot-assisted laser treatment system is composed of a commercial robot and various sensors attached at the end-effector. The system could detect an arbitrary shaped target in red and can perform uniform distribution of laser delivery on the area. Localization-error test and spots-per-area tests were conducted to measure the accuracy and reliability of the image processing result. The clinical trial results of the proposed system were studied and its efficacy was compared with that of the physician's treatment result. The physician completed the target area without successfully delivering a sufficient number of shots while the system provided a near to idealistic result. Moreover, the system

had maintained the uniformity of delivery in equal distances, while the physician could not achieve this. Based on this result, the proposed system is expected to be widely used in the field of laser treatment.

References

1. Dierickx CC, Grossman MC, Farinelli WA, Anderson RR. Permanent hair removal by normal-mode ruby laser. Arch Dermatol. 1998;134(7):837-42.

2. Nanni CA, Alster TS. Laser-assisted hair removal: side effects of Q-switched Nd:YAG, long-pulsed ruby, and alexandrite lasers. J Am Acad Dermatol. 1999;41(2 Pt 1):165-71.

3. Nanni CA, Alster TS. Long-pulsed alexandrite laser-assisted hair removal at 5, 10, and 20 millisecond pulse durations. Lasers Surg Med. 1999;24(5):332-7.

4. Lim SP, Lanigan SW. A review of the adverse effects of laser hair removal. Lasers Med Sci. 2006;21(3):121-5.

5. Lanigan SW. Incidence of side effects after laser hair removal. J Am Acad Dermatol. 2003;49(5):882-6.

6. Willey A, Torrontegui J, Azpiazu J, Landa N. Hair stimulation following laser and intense pulsed light photo-epilation: review of 543 cases and ways to manage it. Lasers Surg Med. 2007;39(4):297-301.

7. Desai S, Mahmoud BH, Bhatia AC, Hamzavi IH. Paradoxical hypertrichosis after laser therapy: a review. Dermatol Surg. 2010;36(3):291-8.

8. Geiges ML. History of lasers in dermatology. Curr Probl Dermatol. 2011;42:1-6.

9. Maiman TH. Stimulated Optical Radiation in Ruby. Nature. 1960;187(4736):493-4.

10. Lepselter J, Elman M. Biological and clinical aspects in laser hair removal. J Dermatolog Treat. 2004;15(2):72-83.

11. Anderson RR, Parrish JA. Selective photothermolysis: precise microsurgery by selective absorption of pulsed radiation. Science. 1983;220(4596):524-7.

12. Adrian RM. Pulsed carbon dioxide and erbium-YAG laser

resurfacing: a comparative clinical and histologic study. J Cutan Laser Ther. 1999;1(1):29-35.

13. Kushikata N, Negishi K, Tezuka Y, Takeuchi K, Wakamatsu S. Non-ablative skin tightening with radiofrequency in Asian skin. Lasers Surg Med. 2005;36(2):92-7.

14. Fitzpatrick RE, Rostan EF, Marchell N. Collagen tightening induced by carbon dioxide laser versus erbium: YAG laser. Lasers Surg Med. 2000;27(5):395-403.

15. Ibrahimi OA, Avram MM, Hanke CW, Kilmer SL, Anderson RR. Laser hair removal. Dermatol Ther. 2011;24(1):94-107.

16. Bernstein EF. Hair growth induced by diode laser treatment. Dermatol Surg. 2005;31(5):584-6.

17. Lim HW, Park S, Noh S, Lee DH, Yoon C, Koh W, et al. A study on the development of a robot-assisted automatic laser hair removal system. Photomed Laser Surg. 2014;32(11):633-41.

18. Choi Y, Han H, Shin D, Lim KS, Yu KS. Comparison of the pharmacokinetics and tolerability of HCP1004 (a fixed-dose combination of naproxen and esomeprazole strontium) and VIMOVO(R) (a marketed fixed-dose combination of naproxen and esomeprazole magnesium) in healthy volunteers. Drug Des Devel Ther. 2015;9:4127-35.

19. Park S, Lim HW, Cho M, Lee DH, Koh W, Kim Y, et al. Improvement in Laser-Irradiation Efficiency of Robot-Assisted Laser Hair Removal Through Pose Measurement of Skin Surface. Photomed Laser Surg. 2016;34(1):42-9.

20. Lim HW, Cho M, Lee DH, Koh W, Kim Y, Chung JH, et al. Development of a Novel Automated Hair Counting System for the Quantitative Evaluation of Laser Hair Removal. Photomed Laser Surg. 2016.

21. Lanigan SW. Management of unwanted hair in females. Clin Exp Dermatol. 2001;26(8):644-7.

22. Shapiro J, Lui H. Treatments for unwanted facial hair. Skin Therapy Lett. 2005;10(10):1-4.

23. Koh WaL, H.W., Cho M, Lee DH, Kim Y, Chung JH, Kim S. A Pilot Study on the Evaluation of Physicians' Laser Delivery Performance Using

a Laser Beam Detection Kit. Photomed Laser Surg. 2016(Accepted).

24. Gonzalez RC WR. Digital image processing: Prentice Hall; 2008.

25. Canny J. A Computational Approach to Edge Detection. Pattern Analysis and Machine Intelligence, IEEE Transactions on. 1986;PAMI-8(6):679-98.

26. Bradski DGR, Kaehler A. Learning opencv, 1st edition: O'Reilly Media, Inc.; 2008. 450 p.

27. Finkel B, Eliezri YD, Waldman A, Slatkine M. Pulsed alexandrite laser technology for noninvasive hair removal. J Clin Laser Med Surg. 1997;15(5):225-9.

28. Campos VB, Dierickx CC, Farinelli WA, Lin TY, Manuskiatti W, Anderson RR. Hair removal with an 800-nm pulsed diode laser. J Am Acad Dermatol. 2000;43(3):442-7.

29. Handrick C, Alster TS. Comparison of long-pulsed diode and long-pulsed alexandrite lasers for hair removal: a long-term clinical and histologic study. Dermatol Surg. 2001;27(7):622-6.

30. Jo SJ, Kim JY, Ban J, Lee Y, Kwon O, Koh W. Efficacy and Safety of Hair Removal with a Long-Pulsed Diode Laser Depending on the Spot Size: A Randomized, Evaluators-Blinded, Left-Right Study. Ann Dermatol. 2015;27(5):517-22.

31. Nouri K, Chen H, Saghari S, Ricotti CA, Jr. Comparing 18- versus 12-mm spot size in hair removal using a gentlease 755-nm alexandrite laser. Dermatol Surg. 2004;30(4 Pt 1):494-7.

32. Goldberg DJ, Silapunt S. Hair removal with a combined light/heat based photo-epilation system. J Cutan Laser Ther. 2001;3(1):3-7.

33. Altshuler GB, Zenzie HH, Erofeev AV, Smirnov MZ, Anderson RR, Dierickx C. Contact cooling of the skin. Phys Med Biol. 1999;44(4):1003-23.

34. Dabrowski M, Dulski R, Zmuda S, Zaborowski P, Pogorzelski C. The use of thermovision camera to observe physiological and pathological conditions of oral cavity mucous membrane. Infrared Phys Techn. 2002;43(3-5):265-9.

35. Marchesini R, Andreola S, Emanuelli H, Melloni E, Schiroli A, Spinelli P, et al. Temperature Rise in Biological Tissue during Nd-Yag Laser Irradiation. Laser Surg Med. 1985;5(2):75-82.

36. Koprowski R, Wilczynski S, Samojedny A, Wrobel Z, Deda A. Image analysis and processing methods in verifying the correctness of performing low-invasive esthetic medical procedures. Biomedical Engineering Online. 2013;12.

Abstract in Korean

본 연구는 레이저 제모 시술에 로봇 기술을 응용하여 시술을 자동화 함으로써 시술자들을 돕고 균일하고 정밀한 레이저 조사를 구현함으로서 시술 받는 사람들에게 향상된 의료 시술을 제공할 수 있는 시스템 개발에 관한 연구이다.

레이저 제모 시술에서 '균일한 레이저 조사'는 최적의 레이저 치료 결과에 위해 필수적이고 아직까지 이를 실현시킬 수 있는 신뢰적인 방법이 없는 상황이다. 제모를 포함한 레이저 치료의 대다수는 '선택적인 광 열 분해 작용' (selective photothermolysis)의 원리를 적용한 방법이며, 이는 빛의 파장, 지속 시간, 조사량을 조절 함으로써 실현이 가능하고, 주변의 조직세포에 대한 영향을 최소화 하면서 목표로 하는 조직세포만을 선별적으로 손상시킨다. 그러므로 레이저가 조사 되지 않은 부분(누락)은 영향을 받지 않고, 효과가 떨어지며, 과다한 조사(중복)가 이루어진 부분은 부작용이 일어날 수 있다.

의사들의 실력을 평가하는 임상시험 결과, 의사들은 균일한 레이저 치료결과가 필요로 하는 만큼의 레이저 조사 횟수를 채우지 못하고 치료를 끝마쳤다. 또한, 레이저 조사 실력을 분석한 결과, 누락에 신경을 쓰면 중복이 일어나고, 중복에 신경 쓰면 누락이 발생하였다.

레이저 시술 작업이 육안상 쉬운 작업으로 보일 수 있으나 실상은 그렇지 않다. 클리닉 에서 사용 되는 레이저제모 기기의 hand-piece 는 약 1.5~2.2 kg 에 달하며 사람의 인체 중 등 또는 하반신과 같은 넓은 범위를 시술할 경우 시술시간 이 1회에 3~5시간 정도 소요 되고 영구적 제모시술의 경우 시술을 보통 한달 간격으로 여러 번 받아야 하므로 환자와 의사 모두 피로도가 누적되는 문제점이 있다. 게다가 시술자의 장시간시술은 피로의 누적도 문제이지만 단순반복 작업으로 인한 집중도 저하를 야기 시키며 이는 레이저 조사의 결과로 이루어져 환자들에게 영향을 줄 수 있다. 레이저는 그 특성상 어떠한 흔적을 남기지 않으며, 0.01초 정도를 깜빡이고 사라지므로, 현재 기술로는 레이저가 조사된 부위와 조사되지 않은 부위를 육안으로 판별할 수 없어 시술자가 구체적으로 레이저의 중복 과 누락 부위를 인지 할 수 없다.

따라서 본 연구에서는 6 자유도를 지닌 로봇팔에 상용화된 레이저 치료기기 및 각종 센서들을 부착하였고, 이를 활용하여 균일한 레이저 조사를 가능하게 함으로써 중복과 누락 부위를 최소화 할 수 있고 또 시술을 자동화하여 피로도를 최소화 할 수 있는 '로봇을 이용한 레이저 제모 자동화 시스템' 을 개발 하였다. 또한 영상처리를 통하여 시술자의 레이저 조사 실력에 관한 정보를 정량적으로 분석해주는 '레이저빔 추적 및 트레이닝 기기' 를 개발 하였다.

레이저 제모 자동화 시스템은 시술자가 설정한 일정한 간격의 레이저

조사가 가능하므로 균일한 레이저 조사가 가능하며, 이는 중복율과 누락율을 최소화 할 수 있는 방법이다. 이를 구현하기 위하여 레이저 제모기, 웹캠, 고성능 레이저 거리센서를 6축 로봇팔의 끝단에 장착하였고, 목표물 의 면적 및 거리에 대한 정보는 각각 웹캠 과 레이저거리센서를 통하여 입력 받는다. 입력 받은 영상 및 정보를 토대로 영상처리를 거쳐 목표물에 해당하는 면적에 균일한 레이저 조사를 조사하며, 모니터상의 graphical user interface (GUI) 를 통하여 레이저 조사여부, 완성까지의 조사현황 비율, 조사 횟수 등을 알 수 있다. 본 시스템은 비정형화된 형상(arbitrary shape)의 목표물 검출이 가능하여, 임의로 목표면적을 빨간색 종이로 제작하여 사용 가능하고, 피험자의 신체부위에 직접적으로 그리는 방법도 가능하다. 이를 통하여 본 시스템은 폐곡선 내의 영역에 균일하게 레이저 조사를 시행한다.

개발된 시스템을 토대로 식약처 승인 절차를 거쳐 임상시험을 진행하였고, 피부과 임상의사의 수기 제모와 비교를 통하여, 제모 자동화 시스템의 효율성과 안정성을 입증하였다. 동일한 조사환경하에 제모 자동화 시스템과 임상수기 결과는 각각 49% 및 29% 의 효율성을 보였다. 본 연구에서 개발된 레이저 치료 시스템은 자동으로 치료영역을 검출 하고 치료시간이 더 많이 소요되나 정밀한 간격의 레이저 조사가 가능하여 더 많은 조사를 실현함으로써, 사람이 할 수 없는 균일한

레이저 치료를 통하여 더 높은 효율성을 보여준다.

핵심어: 레이저 치료, 로봇을 이용한 자동화 치료, 레이저 조사 실력, 균일한 레이저 조사,

학번: 2011-23433